BRNO UNIVERSITY OF TECHNOLOGY
VYSOKÉ UČENÍ TECHNICKÉ V BRNĚ

FACULTY OF CHEMISTRY
FAKULTA CHEMICKÁ

INSTITUTE OF MATERIALS SCIENCE
ÚSTAV CHEMIE MATERIÁLŮ

GALVANIC PLATING OF MAGNESIUM ALLOY WITH NI-P BOND COAT
GALVANICKÉ POKOVOVÁNÍ HOŘČÍKOVÉ SLITINY S NI-P BOND COAT

MASTER'S THESIS
DIPLOMOVÁ PRÁCE

AUTHOR
AUTOR PRÁCE

Bc. Martin Zahálka

SUPERVISOR
VEDOUCÍ PRÁCE

Ing. Jaromír Wasserbauer, Ph.D.

BRNO 2019

BRNO UNIVERSITY OF TECHNOLOGY
FACULTY OF CHEMISTRY

Master's Thesis Assignment

Number of thesis:	FCH-DIP1358/2018	Academic year: 2018/19
Institute:	Institute of Materials Science	
Student:	**Bc. Martin Zahálka**	
Study programme:	Chemistry, Technology and Properties of Materials	
Study field:	Chemistry, Technology and Properties of Materials	
Head of thesis:	**Ing. Jaromír Wasserbauer, Ph.D.**	

Title of Master's Thesis:

Galvanic plating of magnesium alloy with Ni-P bond coat

Master's Thesis assignment:

Experimental determination of the lowest possible thickness of the Ni-P coating on the magnesium alloy for use in standard / industrial electroplating bath (copper).
Preparation of multi-layered systems of different thicknesses of individual layers, taking into account the requirements of possible practical use.
Characterization of prepared samples - coating quality, structural and elemental analysis, mechanical properties and corrosion resistance.

Deadline for Master's Thesis delivery: 10. 5. 2019

Master's Thesis is necessary to deliver to a secretary of institute in the number of copies defined by the dean. This assignment is part of Master's Thesis.

- - - - - - - - - - - - - - -	- - - - - - - - - - - - - - -	- - - - - - - - - - - - - - -
Bc. Martin Zahálka	Ing. Jaromír Wasserbauer, Ph.D.	doc. Ing. František Šoukal, Ph.D.
Student	Head of thesis	Head of institute

In Brno, 31. 1. 2019

- - - - - - - - - - - - - - - -
prof. Ing. Martin Weiter, Ph.D.
Dean

Abstract

The aim of this diploma thesis is to find limiting thickness of nickel-phosphorous coating, that can be electroplated by copper without any defects of magnesium alloy substrate, nickel-phosphorous coating or copper film. The theoretical part describes magnesium alloy substrate AZ91 and its corrosion and corrosion resistance. Furthermore, it focuses at detailed description of electroless Ni-P process and copper electrochemical plating process and their comparison. At the end of the theoretical part, the current research of the use of galvanic plating on magnesium alloy is summarized. The experimental part describes the process of preparation of Ni-P and Cu coatings on AZ91 magnesium alloy. Copper electrodeposition was performed on single and double-layer of Ni-P coating. In addition, the effect of pretreatment prior to copper electrodeposition was discussed. A potentiodynamic test was performed to determine the corrosion properties of the specimens. Subsequently, metallographic cuts of individual specimens were prepared and characterization was performed using an optical and scanning electron microscope. Finally, the elemental composition of individual coatings was determined by EDX analysis.

Keywords

AZ91, Magnesium alloy, Corrosion, Ni-P coatings, Electroless deposition, Galvanic deposition, Copper, Potentiodynamic curves

Abstrakt

Cílem této diplomové práce jse najít nejnižší možnou tloušťku nikl-fosforového povlaku, který může být galvanicky pokoven mědí bez defektů na horčíkové slitině, nikl-fosforového nebo měděného povlaku. V teoretické části jsou shrnuty poznatky o hořčíkových slitinách a jejich korozi. Navíc se teoreticá část zaměřuje na popis procesu bezproudého niklování a elektrochemického pokovování mědí a jejich porovnání. Na konci teoretické části je shrnut současný výzkum o elektrochemickém pokovování hořčíkových slitin. V experimentální části byl popsán proces přípravy povlaků Ni-P a Cu na horčíkové slitině AZ91. Na jedné vrstvě a dvojité vrstvě Ni-P povlaku byla provedena elektrodepozice mědi. Navíc byl diskutován vliv předůpravy před samotnou elektrodepozicí mědi. Za účelem zjištění korozních vlastností vzorků byl vykonán potenciodynamický test. Následně byly připraveny metalografické výbrusy jednotlivých vzorků a pomocí světelného a rastrovacího elektronového mikroskopu byla provedena charakterizace. Na konec bylo zjištěno prvkové složení jednotlivých povlaků pomocí EDX analýzy.

Klíčová slova

AZ91, Horčíková slitina, Koroze, Ni-P povlaky, Bezproudá depozice, Galvanická depozice, Měd, Potenciodynamické křivky

ZAHÁLKA, M. Galvanické pokovování hořčíkové slitiny s Ni-P bond coat. Brno: Vysoké učení technické v Brně, Fakulta chemická, 2019. 61 s. Vedoucí diplomové práce Ing. Jaromír Wasserbauer, Ph.D..

Declaration

I declare that the diploma thesis has been worked out by myself and that all the quotations from the used literary sources are accurate and complete. The content of the diploma thesis is the property of the Faculty of Chemistry of Brno University of Technology and all commercial uses are allowed only if approved by both the supervisor and the dean of the Faculty of Chemistry, BUT.

.....
Student's signature

Acknowledgement

I would like to express gratitude to my supervisor at BUT, Faculty of chemistry, Ing. Jaromír Wasserbauer, Ph.D. for his help and guidance throughout this work. In addition, I want to thank Ing. Martin Buchtík, Ing. Leoš Doskočil, Ph.D. for their help with experiments and Ing. Jiří Másílko, Ph.D. for his help with XRD analysis.

Special acknowledgement belongs to my parents for their psychological and financial support during my studies. Finally, I would like to express gratitude to the rest of my family and to all my friends for supporting me.

Contents

1 Introduction

During the past decades interest in magnesium alloys have been increased due to their light weight and simultaneously excellent mechanical and physical properties. Magnesium alloys are one of the lightest construction materials known these days and these alloys may replace other construction materials, such as steel or aluminium in automobile, aviation, telecommunication or electronics fields of industry. Their great physical and mechanical properties, high strength-to-density ratio, electrical and thermal conductivity, high specific strength and anti-shock resistance are resulted from their hexagonal close-packed crystal structures [1, 2, 3].

However, magnesium alloys have some disadvantages, including poor corrosion resistance and electrochemical stability especially in wet environment. Due to their predisposition to galvanic corrosion the electrolytic coating methods can not be used, that are commonly used for coating of construction materials. Therefore, variety of coatings and surface modification were developed in order to increase these drawbacks. Electroless nickel-phosphorous (ENP) plating method is one of them. First ENP patent, which lead to the practical use of these coatings was granted in 1950 and since the interest of these coatings have been increasing [4]. The ENP coatings may be divided into three groups according to phosphorous content - low, medium and high phosphorous coatings [5]. According to phosphorous content in final coating the material properties, such as microhardness, crystallinity, corrosion resistance and wear resistance, may be easily changed, which is main advantage [5].

Electroplating is very popular in indrustry and it has many advantages over electroless plating in terms of lower production cost, higher coating thickness, lower porosity, better corrosion resistance and higher production efficiency. In contrast, the current density is the highest on the edges and thus the coating has not uniform thickness [6].

The objective of this master thesis is to find limiting thickness of low phosphorous electroless nickel coating, that can be plated by copper without any defects of magnesium alloy substrate, Ni-P film or Cu top coating.

Several characterization techniques were used in order to investigate quality and properties of prepared function layers. The structure and element analysis were examined by optical and electron microscopy and energy dispersive X-ray spectroscopy, respectively. Corrosion resistance of coated AZ91 magnesium alloy was determined via potentiodynamic measurements.

2 Theoretical Part

2.1 Magnesium alloys

Magnesium is the lightest of metals used as construction material with a density of 1.738 g·cm^{-3}. The pure magnesium has high specific strength and is able to be welded in controlled atmosphere. However, magnesium has several drawbacks: low elastic modulus, high chemical reactivity and limited corrosion resistance, etc [7]. In order to improve mentioned drawbacks, alloying with other elements are used to produce magnesium alloys. Several alloying elements are listed below.

Aluminium is the most common element, that is used in mixture with magnesium. It improves the specific strength and the hardness of magnesium alloy, simultaneously Al increases its microporosity.

Lithium increases the ductility of magnesium alloy, but decreases its strength. Lithium is only one element, which may decrease the density of magnesium alloy below density of pure magnesium.

Zinc influences the properties of alloys similarly to aluminium. It improves specific strength of alloys and it is usually used with aluminium, that reduces the solubility of Al in Mg.

Manganese is used as adulterant together with aluminium and improves strength of final alloy.

Iron, copper and nickel have detrimental effects on magnesium alloy properties and they are considered as impurities. Even very small concentrations decrease corrosion resistance [8].

2.2 Magnesium alloy AZ91

Alloy referred as AZ91 is most widely used magnesium alloy worldwide due to good castability and great combination of strength, plastic and corrosion properties. AZ91 usually contains 8 - 10 wt.% Al, 0.2 - 1.5 wt.% Zn and 0.15 - 0.5 wt.% Mn.

The microstructure of magnesium alloy AZ91 is depicted in figure 1 and it consists of α-phase (Mg matrix), eutectic α-phase (Al-rich α) and β-phase (intermetallic $Mg_{17}Al_{12}$). The $Mg_{17}Al_{12}$ phase forms fine precipitates near the grain boundary and discontinuous precipitate. The presence of Mg_2Si and Al_xMn_y phases are reasoned by presence of Si and Mn in alloy [9, 10].

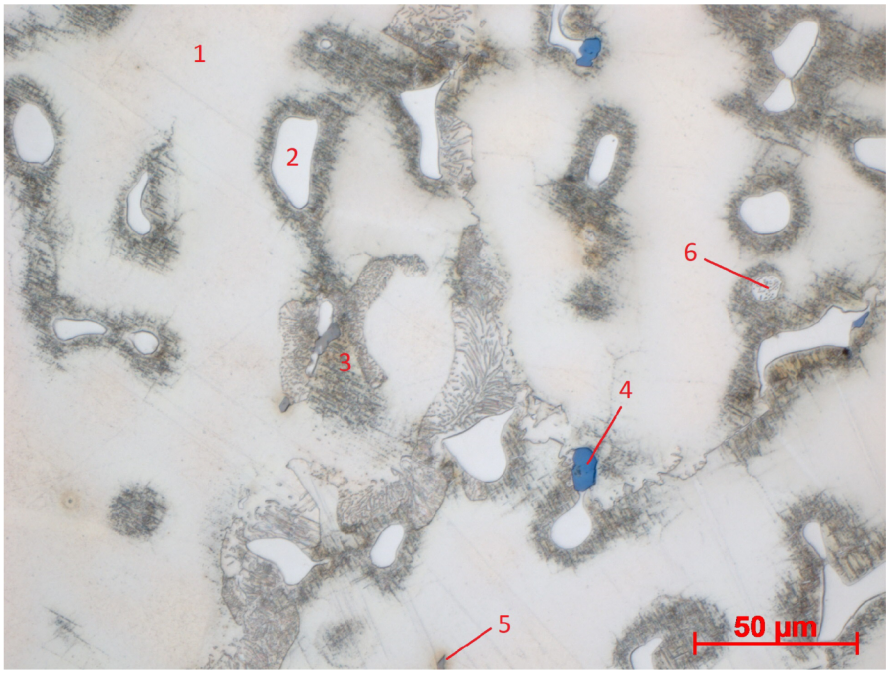

Figure 1: AZ91 microstructure, (1) α-phase (Mg matrix), (2) intermetallic $Mg_{17}Al_{12}$ phase, (3) discontinuous precipitate, (4) Mg_2Si phase, (5) Al_xMn_y phase, (6) eutectic α-phase; 500x magnification

2.3 Corrosion and corrosion resistance

"Corrosion can be defined as an irreversible reaction of a material with the environment, which usually (but not always) results in a degradation of the material or its properties." [11]

Chemical corrosion leads to a chemical reaction in which no electric current arises. The most common type of chemical corrosion is material oxidation in non-conducting environment, such as gases or non-conducting liquids. An oxide layer is formed during oxidation of metals. The oxide layer can act as protective barrier and reduce corrosion rate of a substrate [12].

Corrosion is generally electrochemical redox reaction the surface of material, which can not be stopped. Nevertheless, the corrosion reaction may be reduced by protective barrier on the surface, which leads to slow down of electron transfer from the surface exposed to the corrosive environment to the metal substrate. The oxidation reaction, that takes place on metals is shown in equation (1) [11].

$$M \longrightarrow M^{n+} + ne^{-} \tag{1}$$

On the other hand, the reduction reaction depends on ambient environment. The reduction is different in acidic and aqueous solutions. In acidic solution during the reduction reaction the hydrogen is evolved according to equation (2) [11].

$$2\mathrm{H}^{+} + 2\mathrm{e}^{-} \longrightarrow \mathrm{H}_2 \tag{2}$$

In general the metal may form a soluble cation, soluble anion or an oxide or hydroxide in aqueous solutions. The reduction reaction in aqueous are shown in equations (3 - 5)

$$\mathrm{M} + n\mathrm{H_2O} \longrightarrow \mathrm{MO}_{\mathrm{n}}^{\mathrm{m}-} + 2n\mathrm{H}^{+} + (2n - m)\mathrm{e}^{-} \tag{3}$$

$$\mathrm{M} + n\mathrm{H_2O} \longrightarrow \mathrm{MO}_{\mathrm{n}} + 2n\mathrm{H}^{+} + 2n\mathrm{e}^{-} \tag{4}$$

$$\mathrm{M} + n\mathrm{H_2O} \longrightarrow \mathrm{M(OH)}_{\mathrm{n}} + n\mathrm{H}^{+} + n\mathrm{e}^{-} \tag{5}$$

Corrosion resistance of a single material is always divergent in different environments. In dry atmosphere magnesium forms protective surface oxide layer, but in 1M NaCl solution the corrosion rate drastically increases [13, 14]. Hence, the corrosive environment is very important and have to be considered in material engineering.

2.3.1 Corrosion and corrosion resistance of magnesium and its alloys

In figure 2 is shown Pourbaix diagram, which describes behavior of metals at individual pH and potential values. In the Pourbaix diagram are shown two lines, line *a* and line *b*. Between line *a* and line *b* is defined water stability region. Hence, above line *b* oxygen is developing and below line *a* hydrogen is developing [12].

Generally, in Pourbaix diagram may be found three different regions referred as immunity region, region of activity and region of passivity. In immunity region is Mg stable and any corrosion does not occur. This region is in figure 2 marked as *Mg*. Magnesium is passive at alkaline pH and in figure 2 is marked as $Mg(OH)_2$. Indeed, in alkaline solutions magnesium is covered by magnesium hydroxide, therefore corrosion rate is significantly reduced. In acidic solutions (region of activity) corrosion of magnesium occurs and this region is in figure 2 marked as Mg^{2+}. Lines labeled *0, -2, -4* and *-6* represent activity of Mg^{2+} ions in logarithmic scale [12].

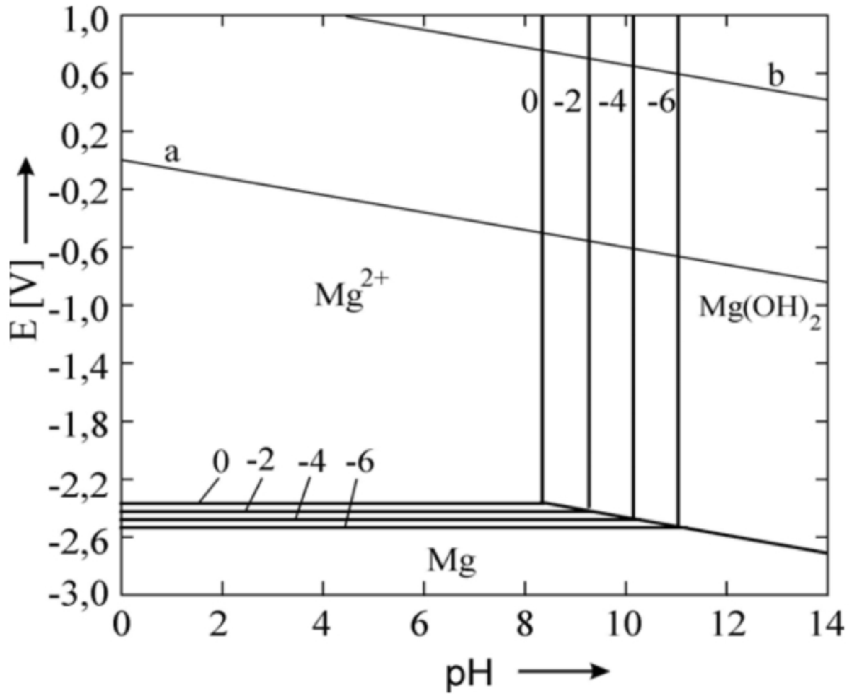

Figure 2: E - pH Pourbaix diagram for Mg [15]

As was mentioned in subsection 2.2, magnesium alloy AZ91 has heterogeneous structure consists of α- and β-phase ($Mg_{17}Al_{12}$). The corrosion potential E_{corr} of α-phase is always higher than that of pure magnesium, due to the presence of aluminium. Moreover, E_{corr} increases linearly with the aluminium content and the corrosion current density I_{corr} also depends on aluminium content. However, E_{corr} of the β-phase is nobler than α-phase. Thus, galvanic coupling occurs between two different phases. Mathieu et al.[16] studied corrosion behavior of main constituent phases of AZ91 in fairly corrosive environment. They observed that increasing aluminium content in α-phase reduces the coupling current between α and β-phase. Moreover, the presence of zinc in α and β-phase were studied. It was observed, that zinc in α-phase does not provide any adjustment for galvanic potential or the current. The couples between α-phase and the zinc rich β-phase show increase of the galvanic current.

Significant role in corrosion resistance of magnesium and its alloys play carefully designed pretreatment process, that can form protective barrier made from oxide/hydroxide layer.

2.4 Treatment processes prior coating application

Carefully designed pretreatment steps play a significant role in order to obtain good protective coatings on magnesium and its alloys. The Mg and its alloys are highly reactive and

therefore they are classified as hard-to-plate materials. Generally, on the surface is formed oxide layer, which has detrimental effects at further metal deposition and prevent good adhesion of the coat to the substrate. Recently, several pretreatment processes have been studied and used in order to prepare high quality ENP coatings [17].

Pretreatment process prior direct ENP deposition includes several important steps: alkaline cleaning, acid pickling and magnesium alloy activation. The purpose of alkaline cleaning is to degrease, remove dirt and other attachments on the surface of specimen. The oxide/hydroxide layer is removed by acid pickling. Furthermore, by acid pickling process the roughness of magnesium alloy surface is increased, thus the adhesion of ENP coating is improved by "interlocking" effect. The activation step is a key to successful direct electroless nickel plating. During activation a conversion coating is formed in order to prevent the corrosion of magnesium alloy [18].

The conventional methods in these day usually need to use toxic chemicals in pretreatment process , such as soaking in a chromium-containing (VI) solution, followed by activation in hydrofluoric acid [18, 19]. As conventional pretreatment process can be viewed the acid pickling in CrO_3 + HNO_3 solution followed by activation in HF at room temperature for certain time [20]. Heakal et al. [21] optimized the conventional pre-treatment process by studying each step effect. They observed, that acid pickling in CrO_3 + HNO_3 solution influences the formation of active sites on AZ91 substrate. Optimum etching time was 60 s in order to obtain a great number of active sites, while longer or shorter time than 60 s causes decrease and partial removal of these active sites. After acid pickling the surface analysis via EDX was done and the results indicate surface layer composed of $MgCrO_4$ and CrOOH. Subsequently, the activation was done by soaking of substrate in H_3PO_4 + NH_4HF_2 solution and EDX surface analysis was performed. The fluoride content in surface layer increases with increasing fluoride ion concentration in activation solution or with decreasing its pH. Indeed, it was found, that fluoride activation process removes all chromium from the alloy surface and replace it with Mg(OH)F and MgF_2.

Current research focuses at replacement of hazardous chemicals in pretreatment steps by environmental friendly non-toxic chemicals. Shao et al [18] studied several acid pickling and activation processes. Authors developed suitable pretreatment process for magnesium alloy electroless nickel plating. The acid pickling was done in solution of H_3PO_4 and HNO_3 (c = 25 ml/l). For activation were used solutions of NH_4F (30-50 g/l) and $NH_4H_2PO_4$ (80-100 g/l) and films consist of MgF_2 and $Mg_2P_2O_7$ were formed, respectively. MgF_2 layer is insoluble in plating bath and it enhance the corrosion resistance of AZ91. Whereas, $Mg_2P_2O_7$ conversion film is dissolved and replaced by electroless nickel coating. The corrosion properties were then investigated by test of electrochemical performance. It was found, that corrosion potential was improved to 1.1 V with a significant reduction of corrosion current.

Singh et al. [22] investigated completely non-fluoride and non-Cr^{6+}/Cr^{3+} processes prior direct electroless nickel plating. These processes were based on the formation of the dense and low soluble oxide/hydroxide, metal carbonate and phosphates on the AZ91 surface. It

was achieved by immersing the AZ91 in (a) lactic acid (25 ml/l) followed by NaOH (b) NaOH + Na_2CO_3 (25 g/l) (c) $NiCO_3$ followed by Na_2CO_3 + Na_2SiO_8 solution (d) H_3PO_4 (8 ml/l) solution followed by the pore sealing in NaOH at 80 °C (e) $Ce(NO_3)_2 \cdot 6H_2O$ + H_2O_2 solution followed by Na_2CO_3 + Na_2SiO_8 solution. The pretreatment processes (c)-(e) enabled the plating to continue for longer duration, without any degradation of the bath. The duplex ENP coatings, with pretreatment repeated in between the two layers, were prepared. The ENP coating on magnesium alloy pretreated by process (a) and (b) did not detach from the surface during deposition and appear visually adherent. Unfortunately, the coating exfoliated after potentiodynamic polarization test, most likely due to penetration of test solution through pores in the coating. Hence, process (c) was developed in order to increase adhesion of ENP coating. Furthermore, due to pretreatment in $NiCO_3$ solution the early nucleation occured and deposition rate increased. The corrosion potential E_{corr} of the ENP was shifted towards noble direction from -1401 mV of the bare substrate up to -346 mV for ENP duplex coating. Also, the corrosion current density decreased from 47 μAcm^{-1} for as received AZ91 alloy to 2.15 μAcm^{-1}, which is the lowest value obtained in this research. Pretreatment processes (d) and (e) show similar trend of increasing corrosion resistance to that observed after the process (c). However, the adhesion strength was found higher using the process (d) and even higher using the process (e). The results were then supported by electrochemical impedance spectroscopy (EIS).

2.5 Electroless nickel - phosphorous coatings on magnesium alloys

Electroless plating is an auto-catalytic process of metal deposition on a substrate. Metal ions in solution are reduced by reducing agent in the bath and metal film is formed on the substrate surface as illustrated in figure 3. The application of electroless nickel has been widely increasing in many industries due to its unique properties, including corrosion and wear resistance. The main advantage is that properties of ENP coatings may be tailored for necessary applications by changing plating parameters and post heat treatment. Electroless plating can be used to prepare metal deposits on conductive even non-conductive materials, such as ceramics or plastics.

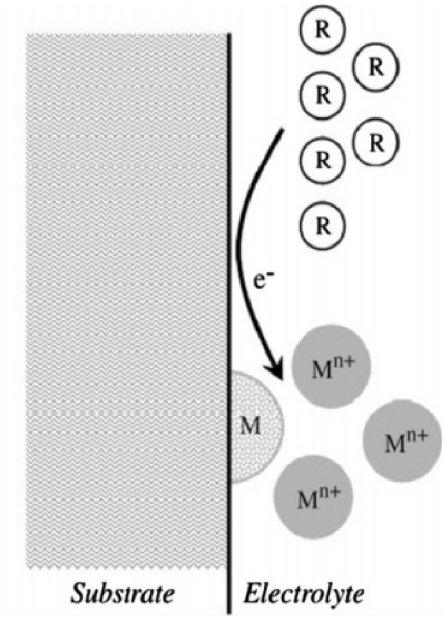

Figure 3: An electroless deposition process with reducing agent R as the source of electrons [23]

Electroless deposition of nickel - phosphorous films is generally oxidation reduction reaction, as can be seen in equations (6, 7). Nickel is reduced from solution by reducing agent and its deposited on adjusted substrate together with phosphorous.

$$Ni^{2+} + 2e^{-} \longrightarrow Ni^{0} \tag{6}$$

$$H_2PO_2^{-} + H_2O \longrightarrow H_2PO_3^{-} + 2H^{+} + 2e^{-} \tag{7}$$

The phosphorous content in final coating may be easily controlled by changing pH, temperature, agitation and solution composition. ENP coatings can be sub-classified into three groups according to P content: low, medium and high phosphorous coatings. The phosphorous content influence the mechanical and physical properties of ENP coatings, e.g. density, hardness, corrosion and wear resistance. In table 1 are referred more differences physical and mechanical properties according to P content in ENP.

The structure of ENP differs from microcrystalline structure, mix of microcrystalline and amorphous structure or simply amorphous structure. With increasing phophorous content the structure is changed from crystalline at low phosphorous level to amorphous nature at high P content. Due to absence of well-defined crystal structure the intergranular corrosion is eliminated and thus corrosion resistance of high phosphorous coatings is higher [23, 24].

The density is inversely proportional to P content in coating. The density of pure nickel is 8.9 g/cm^3, whereas the density of ENP varies from 8.6 to 7.8 g/cm^3 as can be seen in table 1. As well as density, the melting temperature is decreasing linearly with increasing P content. For instance, the melting temperature of pure nickel is 1455 °C, but the ENP deposits containing 11 % P have melting point 880 °C [23, 24].

Hardness of electroless nickel deposits may be varied over wide range. The hardness depends on phosphorous content in deposits and typical hardness values can be found in table 1. In order to increase hardness of deposits, the post heat treatment process can be attached. The post heat treatment process is dependent on treatment time and temperature. The hardness of heat treated deposits can rise up to 1050 HV. The heat treatment process is described in subsection 2.5.4 in more details [23, 24].

Table 1: Physical and mechanical properties of Ni-P coating with different P content [23]

	3-4 % P	6-9 % P	10-12 % P
Structure	Microcrystalline	Microcrystalline and amorphous	Amorphous
Internal stresses [MPa]	-10	+40	-20
Melting temperature [°C]	1275	1000	880
Density [g/cm^3]	8.6	8.1	7.8
Thermal conductivity [W/cm·K]	0.6	0.05	0.08
Tensile strength [MPa]	300	900	800
Elongation [%]	0.7	0.7	1.5
Modulus of elasticity [MPa]	130	100-120	170
Hardness [$HV_{0.1}$]	650	620	520

2.5.1 Composition of nickeling bath

The composition of nickeling bath is very complex system and it is very important to know exact composition. By changing the composition of bath is able to control the chemical and physical properties of ENP coatings. Typically, the ingredients of nickeling bath are a nickel compound, a reducing agent, a complexing agent, an accelerator, a stabilizer, acid/base, buffer and wetting agent [25, 26].

As the source of nickel cations are used nickel sulphate, nickel chloride or nickel acetate. The nickel sulphate is mostly used due to the drawbacks of nickel chloride and acetate. The chloride ions may cause corrosion of substrate during electroless plating of aluminium or aluminium alloys. The high price of nickel acetate restricted its application and in comparison with nickel sulphate has not been observed any improvement [23, 25].

Sodium hypophosphite, amino boranes, sodium borohydride and hydrazine have been commercialized as great reducing agents in electroless deposition of nickel. The electroless

nickel is deposited simultaneously with another element depending on which reducing agent is used. Hydrozine bath has been used in order to develop the high purity nickel film (97 - 99 %). Amino boranes and sodium borohydride produce coatings with boron content up to 10 wt.%. Sodium hypophosphite is usually used due to its low price and great corrosion resistance beside pure Ni and Ni-B coatings [23, 25].

The complexing agents prevent the decomposition of nickeling bath, control the amount of free nickel cations in the solution and control the reaction on catalytic surface. Carboxilic acids or their salts are used as complexing agents in acidic baths, while sodium dihydrogen phosphate is used in alkaline baths. Their function is also buffer the solution and slow down the precipitation of nickel phosphite [23, 25].

In order to increase the rate of deposition are often added the accelerators to the plating solution. Accelerator's main function is activation of $H_2PO_2^-$ and make P-H bond in hypophosphite weaker [26].

The function of stabilizers is to prevent the undesirable reactions in solution and bath decomposition. The electroless nickel deposition may work without stabilizers, but the spontaneous bath decomposition may happen during plating, which is accompanied by hydrogen evolution and formation of nickel precipitates. The stabilizers should not influence the electroless deposition process and final quality of coating. Thiourea is usually used as stabilizer and its concentration should not exceed 0.1 mg/l otherwise the deposition reaction may stop [23, 25].

The effect of wetting agents as component of plating bath has been extensively studied. Surfactants are added to improve wettability of substrate and reduce the interfacial tension between evolved hydrogen bubble, substrate and plating solution [27]. It was found that wetting agents, such as anionic and cationic surfactants, decrease surface roughness, increase microhardness and deposition rates of electroless nickel. In addition, surfactants increase the deposition rate of phosphorous, thus increase the P content in final Ni-P coating [28].

Also, it is very important under what condition is nickel-phosphorous layer formed. These conditions include bath temperature, pH, composition and age. These conditions are discussed in next subsection.

2.5.2 Effect of bath parameters on deposition of Ni-P coatings

The deposition of nickel-phosphorous coatings is affected by several factors such as bath temperature, pH, age and portion of Ni^{2+} and $H_2PO_2^-$. These factors influence the deposition rate, microstructure, porosity of deposits, thus wear and corrosion resistance [25, 29].

Usually chemical reactions are affected by temperature. The temperature has mainly influence on deposition rate of electroless deposition reaction. In figure 4 (right) can be seen that deposition rate exponentially increases with increasing temperature at all pH values. Acidic nickeling baths operate at temperature range of 85 - 95 °C, whilst alkaline baths need

less energy and they operate at temperature range of 50 - 60 °C. Hence, the alkaline baths are more suitable for plating of non-conducting materials, such as plastics [25, 26, 29].

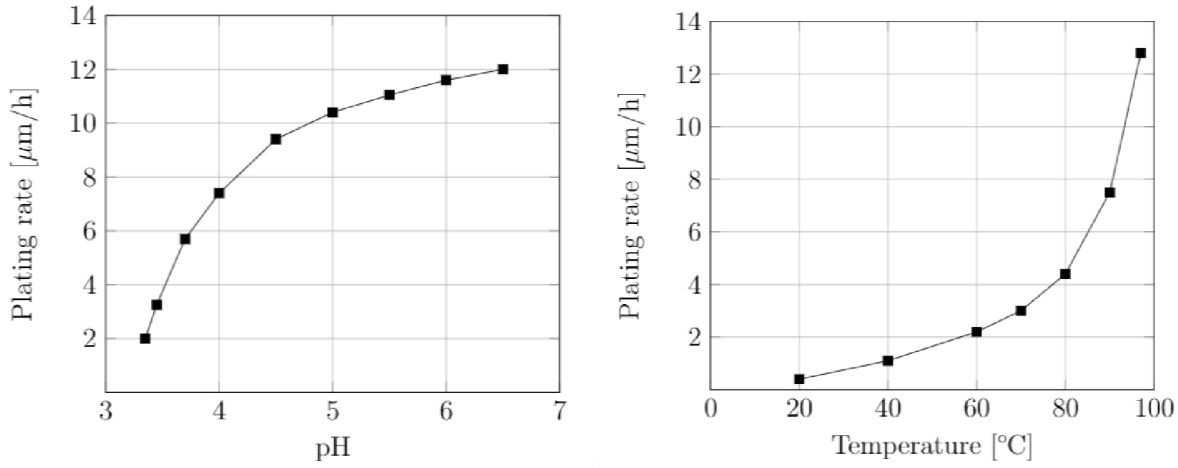

Figure 4: The effect of bath pH and temperature on the plating rate of electroless nickel [23]

During electroless deposition the H^+ ion concentration increases as can be seen in equation (7). That results in drop of pH, hence the buffer must be present in nickeling bath. Especially, acid baths are more sensitive to pH changes. As can be seen in figure 4 (left), the deposition rate is increasing rapidly from pH 3 to 4.5, while from pH 4.5 to neutral pH 7, the deposition rate is increasing moderately. Below pH 3 the deposition reaction stops. Furthermore, operating pH influences phosphorous content in ENP deposits as can be seen in figure 5. At low pH, the high phosphorous coating are able to prepare up to 14 wt.% of phosphorous, while pH raising leads to lowering of P deposition [26, 29].

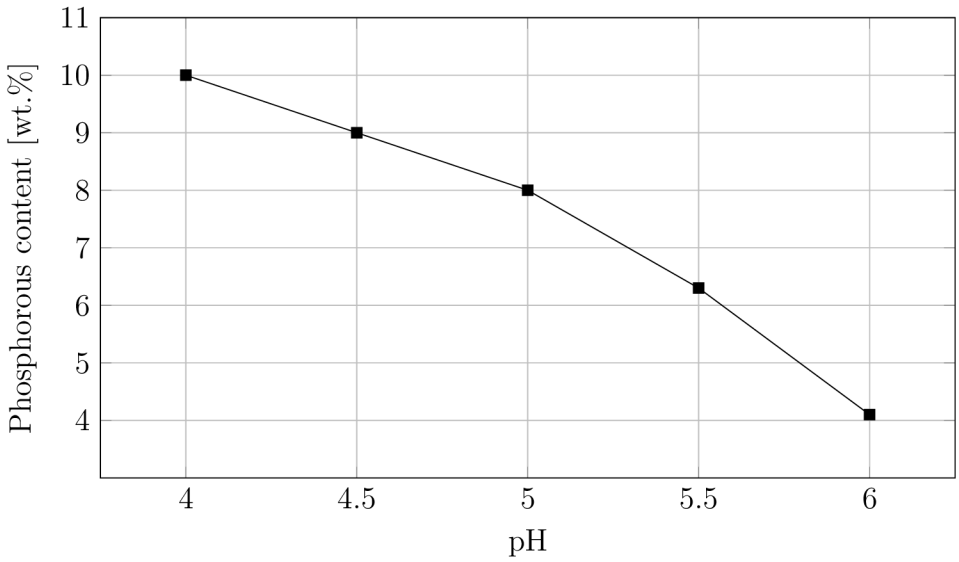

Figure 5: Phosphorous content in ENP coating as a function of bath pH [29]

Nickeling bath do not have infinite life span. The bath age is defined as the number of times the nickel ion is consumed and refilled. This process is referred as "turnover". With increasing number of turnovers, the deposit functional properties become worse, such as corrosion resistance. The deposition rate decreases immediately after first turnover is done and it may decrease as much as 40 % after fourth turnover. Furthermore, the phosphorous content of deposits may rise with increasing turnovers [29].

Nickel ion concentration as portion of Ni^{2+} and $H_2PO_2^-$ are another parameters that influence deposition of ENP. As can be seen in figure 6, optimum $Ni^{2+}/H_2PO_2^-$ portion is between 0.3 and 0.45, while the $H_2PO_2^-$ concentration should be maintained between 0.15 and 0.35 mol/l. If the $Ni^{2+}/H_2PO_2^-$ portion is low and in bath is lack of Ni^{2+} ions, a brownish deposit is obtained and the properties are deteriorated. Whereas, when the $Ni^{2+}/H_2PO_2^-$ portion exceeds 0.6, deposition rate falls down significantly. Moreover, P content in deposits decrease when the portion is high [29].

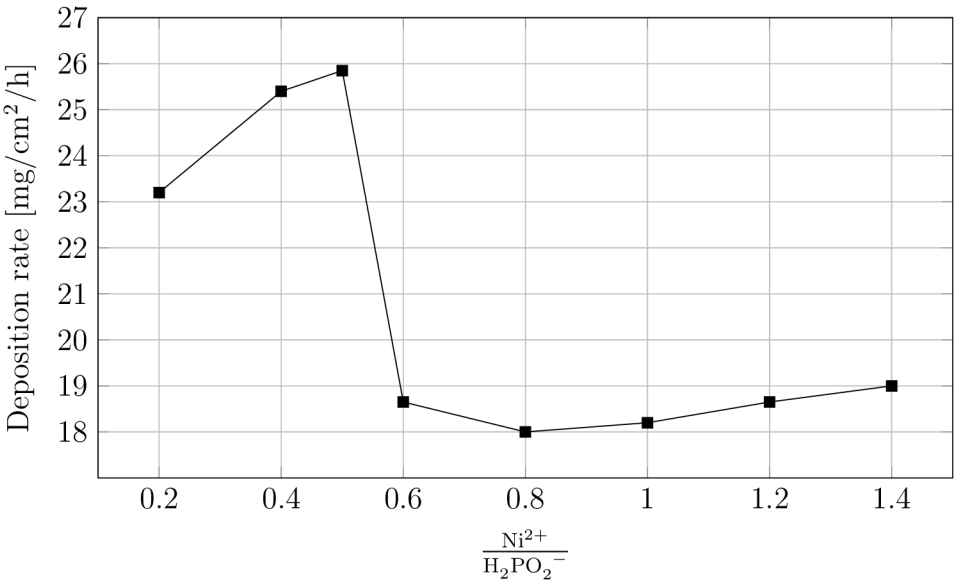

Figure 6: The deposition rate as a function of $Ni^{2+}/H_2PO_2^-$ ratio [29]

2.5.3 Deposition mechanism of ENP coatings

Several deposition mechanism have been proposed, such as mechanism of hydride transfer [30] or adsorption mechanism of $H_2PO_2^-$ and OH^- at catalytically active nickel surface [31]. However, the most promising deposition mechanism of nickel-phosphorous coating was proposed by Cavalloti and Salvago [32] and it was supported by Rondin and Hintermann [33] based on calorimetry. It is assumed that nickel reduction is mediated by donor-acceptor mechanism.

Firstly, hexaaquanickel(II) cation reacts with two hydroxyl ions to form dihydroxotetraaquanickel(II) and two molecules of water according to equation (8).

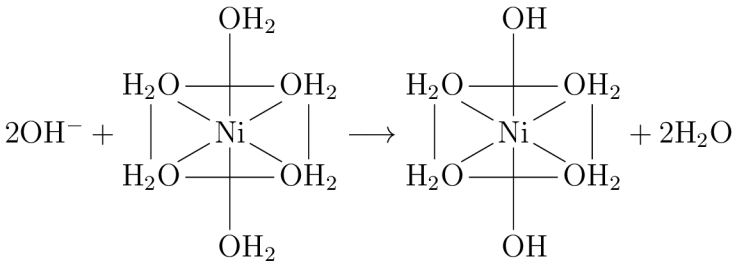

(8)

Dihydroxotetraaquanickel(II) then reacts with $H_2PO_2^-$ to form hydroxonickel(II) cation. $NiOH^+_{ads}$ disposed of four water molecules and it is adsorbed on substrate surface. Another reaction product are monohydrid phosphoric anion and atomic hydrogen as can be seen in equation (9).

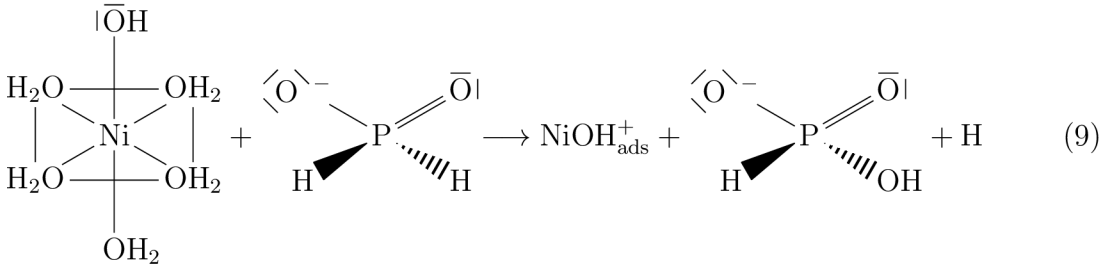

(9)

$NiOH^+_{ads}$ reacts with another molecule of $H_2PO_2^-$ to reduce elemental nickel according to equation (10). During the chemical reaction atomic hydrogen is formed, which then create molecule of gaseous hydrogen equation (11).

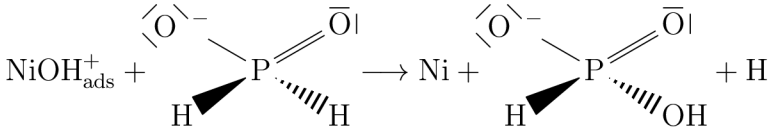

(10)

(11)

2.5.4 Post heat treatment of Ni-P coatings

Nickel-phosphorous coatings may be exposed to high temperature in inert atmosphere. The temperature changes the structure of Ni-P coating and thus improves some of its properties. The post heat treatment increases the hardness of ENP coating significantly up to 980-1050 VPN as can be seen in figure 7. This provides a unique wear and erosion resistance. The optimum temperature for most Ni-P coating is in range of 300 - 400 °C in order to obtain high hardness of coating. Above temperature 400 °C the hardness is decreasing due to formation of larger Ni_3P precipitates [23, 29, 34].

During heat treatment the crystallization of Ni-P coating occurs. The crystallization behaviour of ENP is different for coating having microcrystalline nickel as a major constituent (low and medium phosphorous coatings) and coating containing amorphous structure (high phosphorous coatings). When low phophorous coatings are heated at temperature 200 - 300 °C for 4 h, $Ni_{12}P_5$, microcrystalline Ni and Ni_3P phases are commonly observed. $Ni_{12}P_5$ is metastable phase, which is transformed at higher temperature (400 - 600 °C) to Ni_3P. During heat treatment of medium and high phosphorous coatings at temperature 200 - 300 °C the structure consists of microcrystalline Ni, Ni_3P and several transition phases are usually observed, Ni_5P_4, Ni_2P and $Ni_{12}P_5$. Transition phases are transformed to stable phase Ni_3P above 300 °C and transition temperature is decreasing with increasing phosphorous content in coating. [25, 34, 35]

Despite the increase in hardness, the recrystallization of Ni-P coating is associated with volume shrinkage for medium and high phosphorous deposits. This may result in cracking

and the substrate may be exposed to ambient environment. Thus the corrosion resistance of heat treated Ni-P coatings is reduced especially for high phosphorous deposits [24, 36].

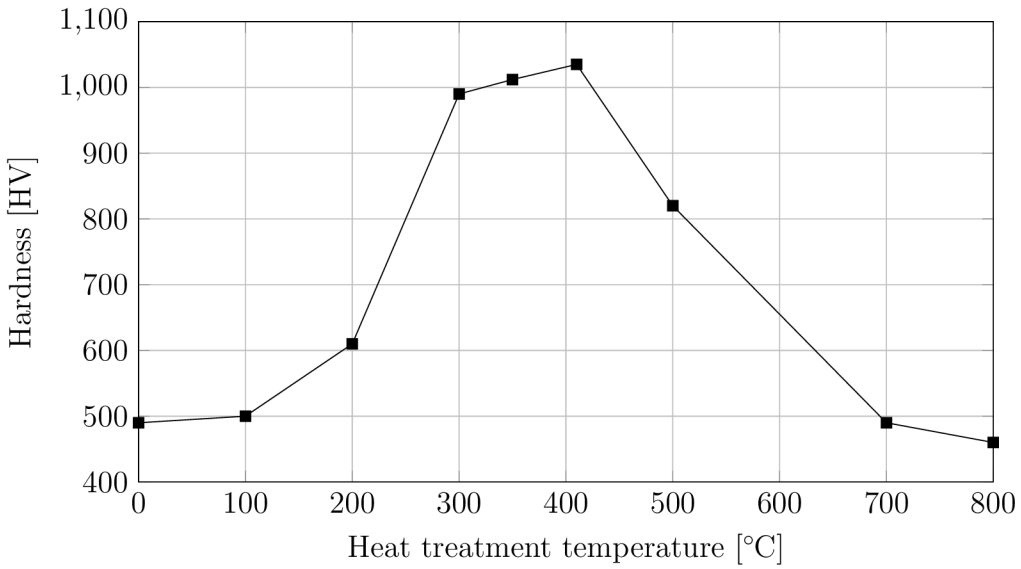

Figure 7: The effect of heat treatment temperature on the hardness of electroless nickel-phosphorous coatings [23]

2.6 Electrolytic deposition of copper on magnesium alloys

Electrochemical plating is a method, that uses electric current to reduce metal cations from solution on electrode surface. An electrochemical plating cell consists of anode, cathode, electrolyte bath and power source, as it is illustrated in figure 8. The part to be coated is connected as cathode, the anode is made of the metal to be deposited on the part. The anode and cathode are immersed in an electrolyte bath, that contains dissolved metal salts in aqueous solution. The dissolved metal ions are reduced at the cathode, simultaneously the anode is dissolving itself in order to keep the concentration of dissolved metal in electrolyte constant. The rate of metal deposition on cathode is equal to the rate of dissolving anode.

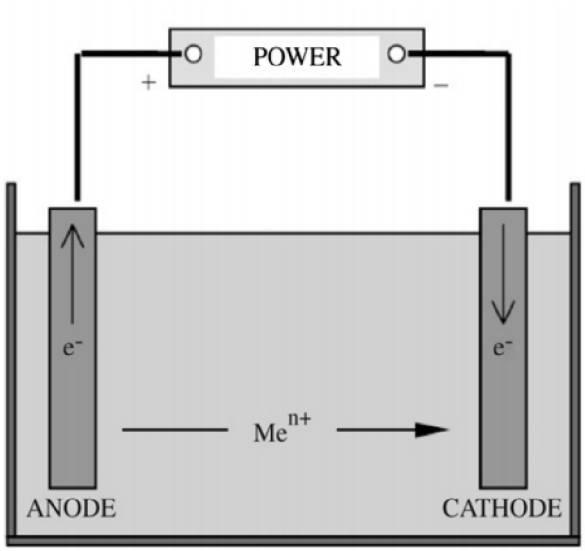

Figure 8: A basic scheme of electrochemical plating cell [23]

Copper is the most common metal plated. The major uses of electroplated copper are plating on plastics, printed wiring boards, automotive bumpers, electroforming or electrorefining. Furthermore, copper is great choice to prepare bond coats. It is able to cover imperfection of substrate and it is inert in most metal plating solutions. Copper electroplating process has a very high plating efficiency and thus it is useful in order to cover hard-to-plate parts. Copper deposits are highly conductive and also act as thermal expansion barrier [6].

Commercially, several types of copper plating systems are available, such as alkaline cyanide and pyrophosphate and acid sulfate and fluoborate systems [37]. Cyanide solutions are suitable for deposition of thin copper films used as and undercoating for nickel and chromium. Due to toxicity and waste treatment problems the cyanide solutions are being replaced by noncyanide pyrophosphate baths. Sulfate and fluoborate acid electroplating solutions are typically used for electroforming and top coats with bright appearance. Fluoborate solutions have capability to deposit copper at very high current densities. However, this solution has minimal commercial usage due to its high price [6].

In experimental part of this thesis is used electroplating bath based on alkaline cyanide solution, so it will be described in more details. Cyanide copper solutions may be typically classified into three types: Strike, Rochelle and high efficiency baths. They differ in bath composition as can be seen in table 2, operating conditions and application. Strike solutions are usually used to apply thin copper undercoating prior deposition of other metals. In order to deposit an intermediate and thick copper coatings Rochelle and high efficiency solutions are used [6].

Table 2: Typical composition of strike, Rochelle and high efficiency copper cyanide solutions [6]

Constituent	Strike [g/l]	Rochelle [g/l]	High efficiency [g/l]
CuCN	22	26	75
NaCN	33	35	102
or			
KCN	43	—	136
Na_2CO_3	15	30	—
NaOH	—	—	15
or			
KOH	—	—	15
$KNaC_4H_4O_6 \cdot 4H_2O$	15	45	—

2.6.1 Composition and function of major constituents of cyanide bath

The plating solutions typically contain cuprous cyanide, free cyanides, additional agents, sodium or potassium hydroxides and carbonates. Cuprous cyanide forms in alkali metal cyanide solution dissociate into Cu^+ and CN^- ions. Furthermore, it forms four stable molecules $CuCN_{aq}$, $[Cu(CN)_2]^-$, $[Cu(CN)_3]^{2-}$, $[Cu(CN)_4]^{3-}$. Deposition is mediated via $[Cu(CN)_2]^-$ and $[Cu(CN)_3]^{2-}$ complexes [6].

As free cyanide is termed the excess of NaCN or KCN, that is not consumed to form $Na_2[Cu(CN)_3]$ or $K_2[Cu(CN)_3]$. Their main role is to provide good conductivity of cyanide bath. Also, free cyanides are important in order to achieve good corrosion of copper anode. If the free cyanide content is too low, insulating film forms on copper anode due to excessive anode polarization [6, 38].

Hydroxides, such as KOH or NaOH, are essential in the plating bath in order to obtain good anode corrosion and provide good conductivity similar to the role of free cyanides. Furthermore, alkali metal hydroxides are used to maintain the pH within the proper range. Some advantages and disadvantages of both, sodium and potassium based processes, have been observed. Solutions based on potassium salts exhibit higher conductivity and higher polarization of cathode. However, solutions based on sodium salts reduce risk of anode passivation [6, 38].

Sodium and potassium carbonate act as a strong buffer and help to keep the pH within a proper range of 10.8 - 11.5. Moreover, it reduces anode polarization, thus enhances the quality of copper film. Generally, carbonates do not have to be added to plating solutions, because they are formed during decomposition of cyanides according to equation (12) [6, 38].

$$2KCN + H_2O + CO_2 \longrightarrow K_2CO_3 + 2\,2HCN \tag{12}$$

Tartrates, sulfur containing organic compounds or water glass are used as additional agents for copper plating. It has been observed that potassium-sodium tartrate ($KNaC_4H_4O_6 \cdot 4H_2O$) has benefit effect to the quality of coating. On the other hand, the organic compounds with sulfur active groups, such as potassium thiocyanate, are used as coating brighteners [6, 38].

2.6.2 Operating conditions and maintenance of solutions

In table 3 can be seen typical operating conditions of strike, Rochelle and high efficiency solutions. Generally, strike solutions are operated at lower temperature than Rochelle and high efficiency solutions. But strike solutions cathode efficiency is approximately 50% lower than that of Rochelle and high efficiency solutions. In order to improve cathode and anode efficiencies of strike solutions $KNaC_4H_4O_6 \cdot 4H_2O$ (Rochelle salt) is used. The higher performance of Rochelle and high efficiency solutions are obtained by controlling pH, increased temperature and higher concentration of CuCN and Rochelle salt [6].

If current density is beyond the limit excessive polarization occurs and insulation film on anode surface is formed. This can cause reduction of anode area or even completely insulate the anode. The effect of copper and free cyanide content variations have been studied. It was found, that copper and free cyanide content variations have little effect on the limiting current density. Furthermore, the variations of pH do not affect limiting current density significantly [6].

Table 3: Operating conditions for strike, Rochelle and high efficiency solutions [6]

Conditions	Strike	Rochelle	High efficiency
Temperature [°C]	40 - 60	55 - 75	60 - 80
Cathode current density [A/dm^2]	0.5 - 4	1.5 - 6.5	1 - 11
Anode current density [A/dm^2]	0.5 - 1	0.8 - 3.3	1.5 - 5
Cathode efficiency [%]	10 - 60	30 - 90	70 - 99
Anode efficiency [%]	95 - 100	50 - 70	—

2.7 Comparison of electrochemical and electroless plating

There are many differences in electrochemical and electroless plating process. Firstly, electrochemical plating uses electric current to reduce metal cation from solution and electroless deposition process uses chemical reaction to reduce metal on substrate by reducing agent. The deposited metal purity also depends on the process, that is used. The electrochemical plating produce metal layer with purity typically greater than 99 %. Whereas, the electroless deposition process produces metal layer with lower purity due to reducing agent is used to reduce metal cations [24].

Nevertheless, the impurities in electroless coating change their structure to obtain coating unique properties. For instance, the electrolytic nickel has crystalline structure, but structure of electroless nickel is dependent on phosphorous content in the final coating and typically with increasing P content the microstructure becomes more amorphous. Thus, the amorphous structures provide better corrosion resistance, but the wear and thermal resistance are reduced [24].

As can be seen in figure 9, the uniformity of electrolytic and electroless coating are very different. The current density during electrolytic plating is the highest on the corners and edges and thus, the thickness of plated metal is the highest on the corners. The electroless deposition process produces deposits with very high degree of uniformity. This huge advantage over electrolytic plating plays significant role in coating of complex parts, such as valves or threaded components [24].

The deposition rate of nickel coating is much lower via electroless plating (5 - 25 μm/h) in comparison with electrolytic nickeling (25 - 180 μm/h). Electroless plating bath is also more demanding for maintenance and it has lower service life. This makes electroless plating process less economical over electrolytic plating. [1, 26]

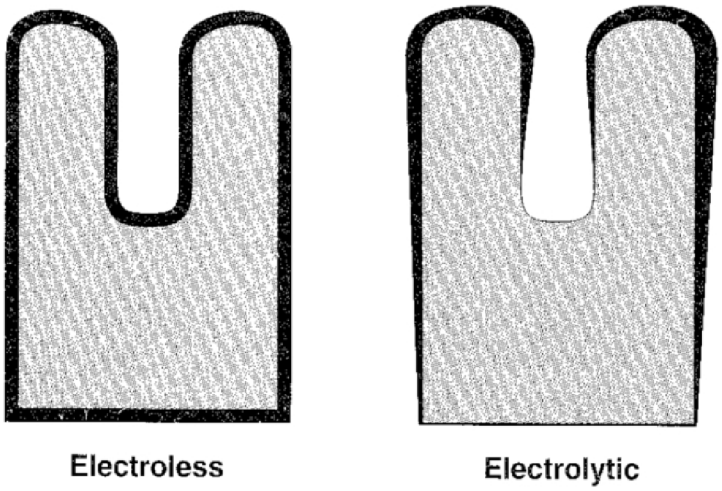

Figure 9: Comparison of coating uniformity in electroless and electrolytic plating [24]

2.8 Current research

2.8.1 Electroplating of Cu/Ag/Cu multi-layer systems on Mg alloy AZ31

N. Van Phuong et al. [39] investigated the corrosion resistance of electrodeposited copper layer on AZ31 magnesium alloy with and without additional silver layer. The samples were pretreated by activation in HF solution and zincate conversion coating. The zincate layer decreases the reaction rate between the substrate and pyrophosphate ions from the plating solution and it prevents the formation of non-conductive magnesium oxide/hydroxide layer. Afterwards, copper single-layer coating an multi-layer Cu/Ag, Ag/Cu, Cu/Ag/Cu were prepared on AZ31 magnesium alloy. The Cu single-layer has nodular structure with crevices between individual nodules. Additional Ag layer covers both the nodules and crevices. The morphology of second Cu layer deposited on Cu/Ag layers shows smooth surface with fine particles. This indicates that Ag layer provides many nucleation site and thus denser Cu top coat can be deposited.

Corrosion resistance was then determined by potentiodynamic test and immersion test. The corrosion potential and current density were determined from potentiodynamic curves. The coated Mg alloy AZ31 showed much more positive corrosion potential than bare AZ31 except single-layer Cu coating. The Cu single-layer shows almost 4 times higher corrosion current ($74 \cdot 10^{-5}$ Acm^{-2}) than bare AZ31 substrate ($19.6 \cdot 10^{-5}$ Acm^{-2}). It is caused by poor structure of first Cu layer and galvanic coupling effect between AZ31 anode and Cu cathode. The best corrosion resistance was recorded for the sample coated with Cu/Ag/Cu multi-layer system with corrosion potential of -0.23 V vs. SCE and corrosion current of $0.92 \cdot 10^{-5}$ Acm^{-2}. Immersion test was performed in 0.5 M NaCl solution and it shows that the pit density and pit size is different for the different coating systems. The Cu single-layer samples and sample with Cu/Ag double-layer show the highest pit density, but pits are small. In contrast, the triple-layer Cu/Ag/Cu samples show the formation of large pits, but their density is small. This corresponds to amount of imperfections in coatings. The increasing pit size is due to galvanic corrosion between the anodic AZ31 substrate and the cathodic Cu/Ag coating [39].

2.8.2 Environmental friendly Ni electroplating on AZ91 coated with Ni-P

C. Singh et al. [40] investigated electroplating of nickel on magnesium alloy AZ91 with and without prior environmental friendly pretreatment. Authors examined nickel electroplating on bare AZ91 substrate and pretreated AZ91. The Mg alloy AZ91 substrate was subjected to the various pretreatment processes. First process *P1* consists of pickling in acid solution of $NiCO_3$ for 30 s followed by an immersion in Na_2CO_3 + Na_2SiO_8 for 3 min. Second process *P2* consists of pickling in H_3PO_4 solution for 30 min followed by an immersion in NaOH for 2h. Despite pretreatment processes, the electroplating on the bare or pretreated surface of AZ91 was not possible and led to the bath degradation or coating delamination.

In order to improve the the quality and adhesion of Ni top coat, single-layer of nickel-phosphorous coating (∼10 μm) was introduced on the pretreated AZ91 substrate. However, Ni-P layer did not allow a sustained nickel electrodeposition and delamination of Ni coating occured. This is due to an incomplete coverage of the substrate with Ni-P and presence of small pores and gaps. The plating solution is able to reach the AZ91 substrate through pores and cause the galvanic corrosion. Afterwards, double-layer Ni-P coating (∼20 μm) was prepared. By applying the second Ni-P layer, the coating turned into compact with minimal defects. Subsequent nickel electroplating was found feasible on double-layer Ni-P for duration of 5 min (∼5 μm). By increasing the deposition time to 30 min, the quality of Ni layer was decreased, cracks were formed and resultant coating started to detach. To improve the sustainability of the coating process for longer duration, the electroplating bath temperature was increased from 25 °C to 70 °C and nickel layers with thickness of 10, 15 μm were developed [40].

The corrosion resistance was determined via potentiodynamic polarization test in 0.5 % NaCl solution. The nickel electroplating process on pretreated AZ91 by *P1* and *P2* with duplex Ni-P coating specimens carried out at 25 °C showed poor corrosion resistance according to the high corrosion current density (i_{corr}) value of 18.8 and 13.3 μAcm^{-2}, respectively. It is much higher than the i_{corr} ∼ 7.9 and 7.7 μAcm^{-2} obtained from the 5 μm thick nickel layer using *P1* process pretreatment at 50 and 70 °C, respectively. Identical trend can be seen using pretreatment *P2* process, but the i_{corr} values are significantly lower (∼ 4.7 and 1.4 μAcm^{-2} at bath temperatures of 50 and 70 °C). The lowest i_{corr} values were observed for AZ91 pretreated by *P2* process with double-layer Ni-P electroplated at bath temperature 70 °C with thickness of 5, 10, and 15 μm ∼ 1.4, 1.0 and 0.8 μAcm^{-2}, respectively.

3 Thesis Objectives

Experimental determination of the lowest thickness of Ni-P bond coat on magnesium alloy to use standard/industrial galvanic bath (copper). Preparation of multi-layered systems with different thicknesses of individual layers. taking into account the requirements of possible practical use. Characterization of prepared samples - coating quality, structural and elemental analysis, mechanical properties and corrosion resistance.

4 Experimental Part

4.1 Chemicals and materials

Chemicals and materials, listed below, were used in experimental part of this diploma thesis.

2-Propanol	(VWR Chemicals, Technical $\geq$ 98 %)
Acidic bath	(FCH BUT research, Laboratory of metals and corrosion)
Alkaline bath	(FCH BUT research, Laboratory of metals and corrosion)
Distilled water	(FCH BUT, conductivity $< 0.7\ \mu s \cdot cm^{-2}$)
Electroplating bath – copper	(CUPRALYTE^{TM} 1545)
Epoxy resin	(AKASEL Aka-Resin liquid)
Epoxy resin hardener	(AKASEL Aka-Cure slow)
Ethanol	(Distillery Kolín, min. 96 %)
Nickeling bath	(FCH BUT research, Laboratory of metals and corrosion)

Magnesium alloy AZ91 was used as substrate for ENP coating. Composition of AZ91 was determined by glow-discharge optical emission spectroscopy (GDOES) and it is shown in table 4 [41].

Table 4: Composition of magnesium alloy AZ91

Element	Al	Zn	Mn	Si	Zr	Mg
Content [wt.%]	8.8	0.81	0.32	0.01	0.01	90.05

4.2 Preparation of magnesium alloy specimen

The specimens were made of AZ91D magnesium alloy and the testing specimens were cut by metallographic saw Struers Discotom-6 into rectangular pieces with dimensions of $30 \times 30 \times 6$ mm. Into edge were then drilled 1 mm holes, that serves to hang the sample. Subsequently, the samples were grinded by silicon carbide grinding paper of 400 - 1200 grit to ensure a uniform roughness. Grinded samples were washed by distilled water, isopropanol and dried by hot air.

4.3 Electroless Ni-P deposition

Grinded samples were submerged in alkaline cleaning bath for 20 min at temperature 60 °C. After 20 min, samples were washed by distilled water, isopropanol and dried by hot air flow. Subsequently, the samples were submerged in acid pickling bath for 5 s, washed by distilled water, isopropanol and dried by hot air. After acid pickling, the samples were immersed in nickeling bath for 15 - 180 min. The samples with single-layer Ni-P bond coat was labeled as $AZ91_{SEN}$.

The duplex (two) layers, each of ∼6 μm (total 12 μm) thicknesses (for an entire period of 90 min) in the same bath (composition, pH, temperature) were prepared. The duplex Ni-P layers on the AZ91 was obtained by applying pretreatment process in between the two layers. The specimen was labeled as $AZ91_{DEN}$.

4.4 Electrolytic copper plating

Samples coated by electroless nickel were connected as a cathode and immersed in plating bath solution. For the first 15 minutes the electric current was set to 0.02 A in order to deposit initial copper layer. After 15 minutes the electric current was set to 0.1 A for 60 min and 150 min in order to prepare Cu layer with thickness of 10 μm and 25 μm, respectively. The plating times were calculated from Faraday's law, equation (13)

$$t = \frac{d \cdot z \cdot F \cdot A \cdot \rho}{I \cdot M}, \tag{13}$$

where t is time, d is coating thickness, z is the valency number of ions of the substance, F is Faraday's constant (96485 C $\cdot$ mol^{-1}), A is sample area, I is electric current, M is molar mass.

4.5 Corrosion resistance measurement

4.5.1 Potentiodynamic polarization of coating

Potentiodynamic test was performed at potentiostat Bio-Logic v SP 300. Experimental values of corrosion potential E_{corr} and corrosion current I_{corr} were measured by apparatus consists of saturated calomel electrode (SCE) as reference electrode, specimen as working electrode and platinum mesh as counter electrode. The potentiodynamic test was carried out in 0.1 mol $\cdot$ dm^{-3} solution of sodium chloride in range of -100 mV to 200 mV at a constant voltage scan rate of 1.0 mV/s.

4.6 Coating characterization

4.6.1 Metallographic cut preparation

Metallografic cut was prepared in order to characterize specimen. Testing specimen was appropriately sawed using a Secotom-50 metallographic saw. Subsequently, it was suffuse by epoxy resin and cured at laboratory temperature for 24 h. Cured sample was grinded at automatic grinder Tergamin-25 using 320, 1200, 4000 grit silicon carbide grinding paper and polished by 3 μm diamond paste Struers MD-Paste.

4.6.2 Hardness

The hardness of the coating was determined by micro hardness tester LECO AMH55 using Vickers method. Microhardness was measured on perpendicular metallographic cut at 10 gf (gram force) with a duration of 10 s. Similarly, macrohardness of specimen surface was performed at 500 gf (gram force) and 2000 gf with a duration of 10 s. A minimum of 6 indents were made and their average value were reported.

4.6.3 Optical microscopy

Optical microscope Zeiss Axio Observer Z1m was used to characterize substrate, Ni-P bond coat and Cu top coat. Furthermore, thicknesses of individual layers were measured.

4.6.4 Scanning electron microscopy

Sample morphology was observed using scanning electron microscope Zeiss Evo LS-10 fitted with secondary electron (SE) and backscatter electron (BSE) detector. The SEM pictures were taken under following conditions:

- Accelerating voltage — 15 kV
- Working distance — 12 mm
- Magnification — 2300x
- Probe current — 939 pA

Sample composition and element mapping were studied by energy dispersive X-ray spectroscopy (EDX) detector. Measurement deviation of EDX analysis is 0.5 wt.%. Elemental composition was measured under following conditions:

- Accelerating voltage — 15 kV
- Working distance — 12 mm
- Dead time — 50 %
- Number of counts — 700 000

4.6.5 X-ray diffraction

In order to characterize structure of Cu top coat X-ray diffraction analyzer Empyrean Panalytical was used. X-rays were generated via X-ray tube with copper target of wavelength $\sim 1.5426\,\text{Å}$. Measurement was performed with a step 0.013°.

5 Results and Discussion

Magnesium and its alloys are referred as hard-to-plate materials, but using proper pretreatment method electrodeposition of metals can be used. It is one of many potential methods to protect Mg alloy from corrosion. Electroplating has some benefits over other surface treatment methods such as conversion or organic coatings. Metallic coatings provide conductive layer on surface, which is required in many application [39]. Also the electroplating process is cost effective and simple to maintenance in comparison with other deposition techniques. In addition, their simplicity to adopt for industrial application is important. Several metals have been deposited via electroplating process such as copper, nickel or chromium [40]. In this thesis, copper has been chosen for its excellent conductivity and superior corrosion protection. Copper has been deposited from alkaline cyanide bath due to its utilization in industrial practice.

5.1 Galvanizing of AZ91 coated with low-phosphorous Ni-P

Firstly, copper electrodeposition was performed on low-phosphorous Ni-P layer. The deposition times were set to 15, 30, 45, 60, 90 and 120 min, which corresponds to thicknesses of approximately 2, 4, 6, 8, 12 and 16 μm, respectively. Unfortunately, due to the well-defined crystal structure of low-phosphorous Ni-P coating their corrosion resistance is poor. Furthermore, the presence of pores increases the possibility of galvanic coupling between AZ91 substrate and copper top coat. Thus, at all specimens were formed pits and succumbed to corrosion. According to this experiment the low-phosphorous Ni-P coating is not suitable bond coat for subsequent galvanic plating and it was replaced by high-phosphorous Ni-P coating in further experiments.

5.2 Determination of the lowest thickness of Ni-P bond coat

In order to determine the lowest possible thickness of high-phosphorous Ni-P bond coat suitable for copper galvanic plating the six specimens with different thicknesses of Ni-P were prepared. The deposition times of ENP coating were set to 45, 60, 120, 150, 180 and 240 min, which correspond to thicknesses of 6, 8, 16, 20, 24 and 32 μm, respectively. The electric current during electroplating of copper was set to 0.02 A and the copper deposition lasted 15 min. Temperature of plating bath was maintenance at 50 °C.

In figure 10 can be seen photographs of these specimens after copper electrochemical plating. The copper top coat was successfully deposited on all AZ91 specimens coated with different thicknesses of Ni-P bond coat. In figure 10f) can be seen the specimen coated with approximately 32 μm thick Ni-P layer. On the specimen surface were observed corrosion products. However, there is not any reason that specimen with the highest thickness of Ni-P would be corroded. In the case of a lower Ni-P thickness, the intermetallic phase on the AZ91 surface may not be completely covered and hence corrosion may occur. But as can be seen in figure 10a) the specimen coated with 6 μm thick Ni-P was suitable for copper electrodeposition. It was not observed corrosion of AZ91 substrate and plating bath degradation did not occur. Due to the low thickness of Ni-P, the coatings follow the substrate roughness. This was not observed in samples with higher Ni-P coating thickness as can be seen in figure 10b)-f). Based on this experiment, the lowest possible thickness of the Ni-P coating was determined to be 6 μm.

As can be seen the 6 μm thick single-layer ENP provides sufficient corrosion protection of AZ91 substrate prior copper electroplating from cyanide bath of pH = 11. It is in contrast with literature [40], where authors were not able to obtain nickel from electroplating bath (pH = 8) on the $\sim$10 μm thick single-layer Ni-P coated AZ91 substrate. The nickel coating delaminated after 2 minutes. The difference is in pretreatment process. In this work was used pretreatment process developed in previous research at Faculty of chemistry BUT [42]. Using this pretreatment, a high quality Ni-P coating was deposited that did not exfoliate during the electrodeposition of copper, nor did the substrate corrode. This suggests that proper substrate pretreatment prior deposition of Ni-P is very important.

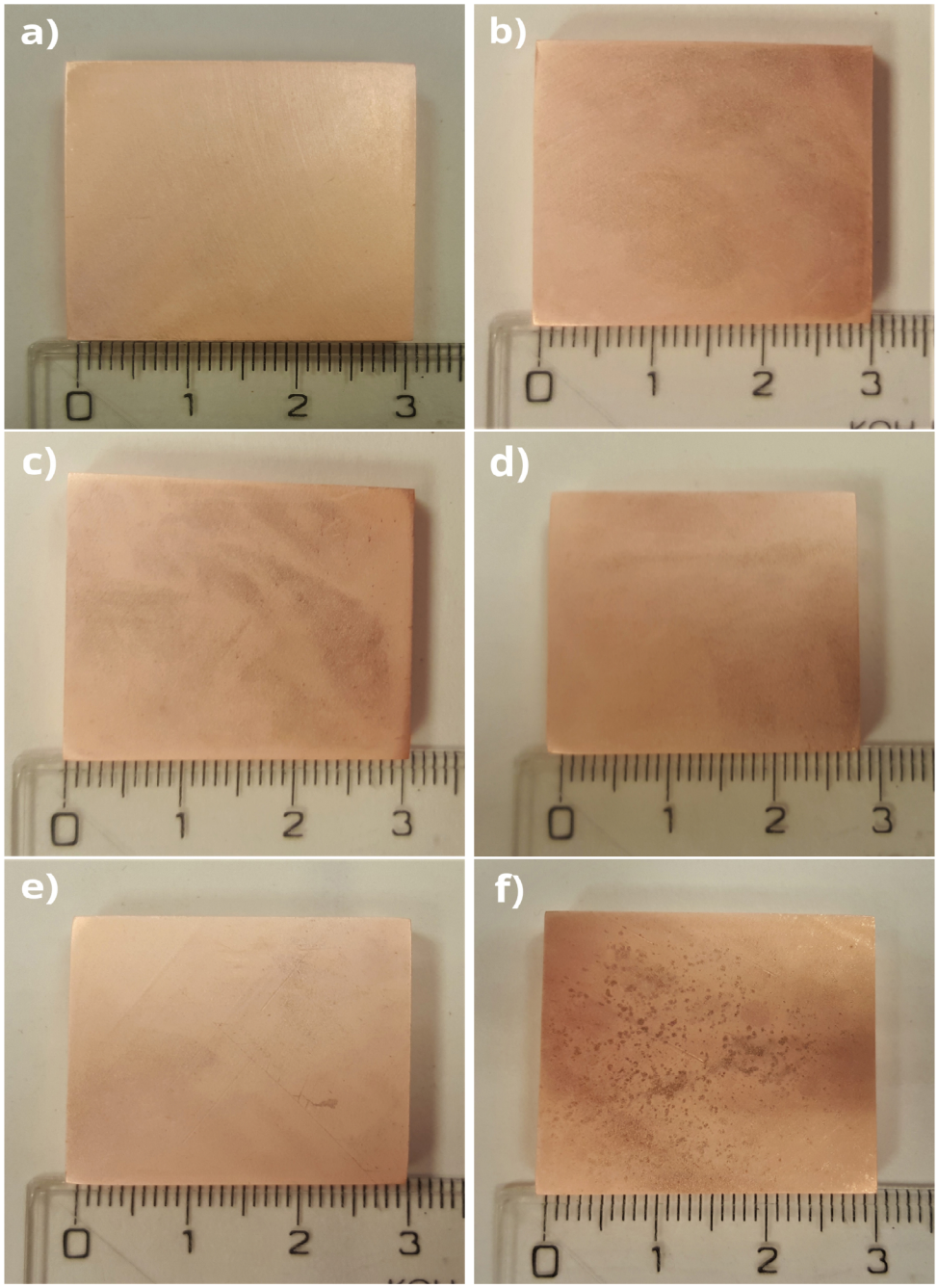

Figure 10: Copper top coat on AZ91 coated with high-phosphorous Ni-P of different thicknesses of a) 6 μm, b) 8 μm, c) 16 μm, d) 20 μm, e) 24 μm and f) 32 μm

5.3 Optimalization of galvanic plating process

Based on previous experiment, the AZ91 was coated with approximately 6 μm thick layer of high-phosphorous Ni-P layer. Electroplating of copper was performed at bath temperature of 50 °C. In order to deposit the initial copper layer the electroplating current was set to 0.02 A and the deposition lasted 15 min, which corresponds to cathode current density value of 0.08 A·dm^{-2}. Subsequently, the current was increased to 0.10, 0.15 and 0.20 A for another 15 min, which corresponds to cathode current density of 0.4, 0.6 and 0.8 A·dm^{-2}, respectively.

It was found, that formation of the initial layer of copper at low current densities is crucial in order to deposit dense copper coating with higher thicknesses and good quality. Furthermore, the effect of higher current densities was studied. In the figure 11 can be seen the copper coating appearance at cathode current density values of 0.4, 0.6 and 0.8 A·dm^{-2}. By increasing the cathode current density from 0.4 A·dm^{-2} (figure 11a) to 0.8 A·dm^{-2} (figure 11c) the surface appearance changed from bright orange surface to dark orange. These dark orange surface areas may be referred as “burnt”. The mechanism of “burnt” areas formation can be explained by lack of copper ions that can be reduced at cathode film, so the electrolytic ”pressure” starts to reducing the hydrogen ions to hydrogen gas. Due to the rapid depletion of hydrogen ions at the cathode film, the pH will rise sharply. In immediate vicinity the concentration of hydroxide ions will increase to the point, that precipitation of copper hydroxide will occur [6].

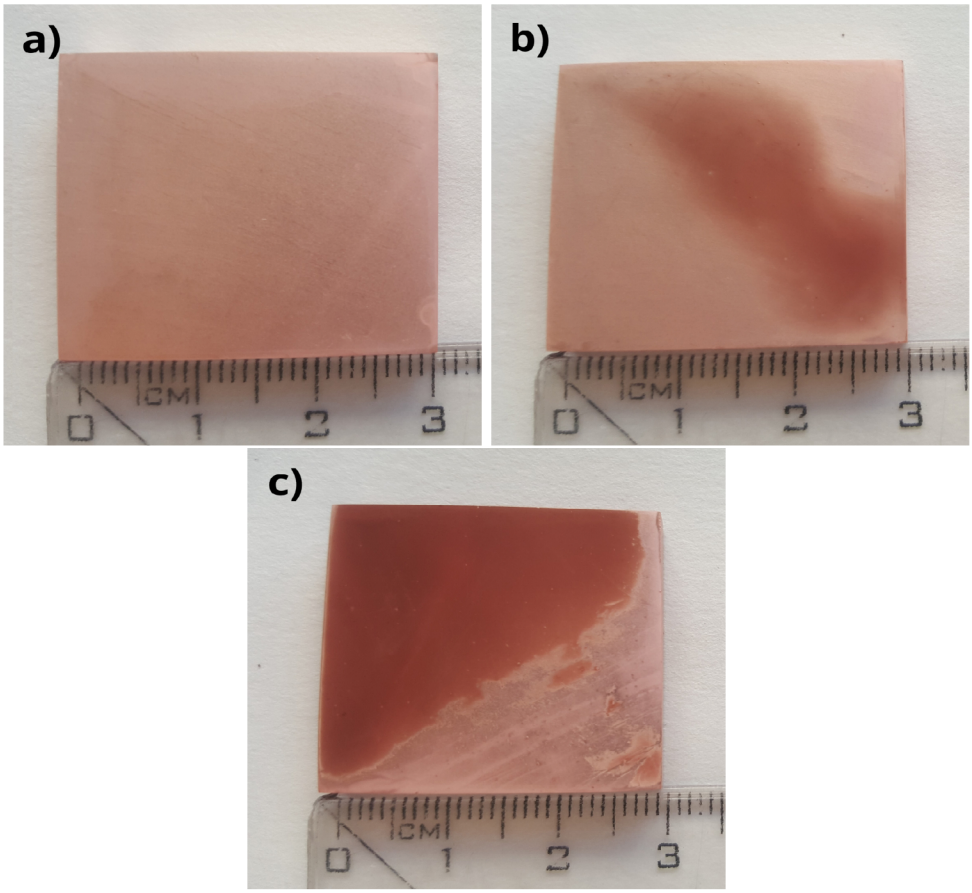

Figure 11: Copper electrodeposition on AZ91 coated with 6 μm high-phosphorous Ni-P bond coat at set cathode current density values of a) 0.4 A·dm^{-2} A b) 0.6 A·dm^{-2} and c) 0.8 A·dm^{-2}

The "burnt" areas were further studied by XRD analysis. In figure 12 can be seen XRD pattern of specimen surface from figure 11c). The copper coating at this specimen was too thin and X-rays penetrated to Ni-P bond coat and AZ91. The peaks with the highest number of counts correspond to diffraction of copper at angles $2\theta \approx 43°$ (plane 1,1,1), $\approx 50.5°$ (plane 2,0,0), $\approx 74°$ (plane 2,2,0) and $\approx 89.9°$ (plane 3,1,1). The other diffraction peaks with lower intensities at angles $2\theta \approx 32.4°$, $2\theta \approx 34.6°$, $2\theta \approx 36.8°$, $2\theta \approx 48.1°$, $2\theta \approx 57.7°$, $2\theta \approx 63.5°$, $2\theta \approx 69.1°$, $2\theta \approx 70.5°$ correspond to diffraction of magnesium zinc compound with formula $Mg_{0.97}Zn_{0.03}$. Unfortunately, the diffraction peaks of Ni-P were not observed. Due to its amorphous structure these peaks are broad and have low number of counts. In "burnt" areas were not observed any diffraction peaks of copper hydroxide as was mentioned above in description of "burnt" areas formation. In figure 13 is shown XRD pattern of specimen $AZ91_{SEN\text{-}Cu25}$. The X-rays did not penetrate the 25 μm thick copper coating and it is used for comparison. As can be seen the highest number of counts is at diffraction at angle $2\theta \approx 43°$ that corresponds to plane (1,1,1). The diffraction peaks at angle $\approx 50.5°$ (plane 2,0,0), $\approx 74°$ (plane 2,2,0) and $\approx 89.9°$ (plane 3,1,1) have very low intensities.

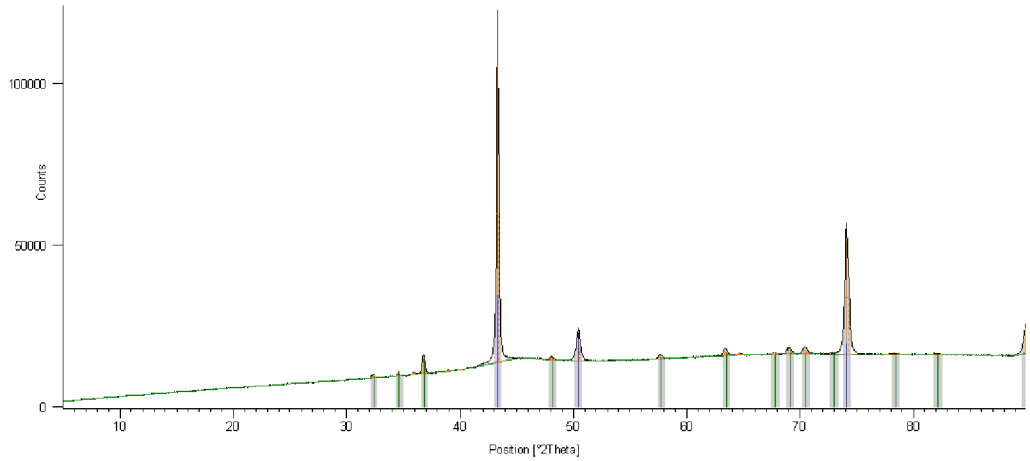

Figure 12: X-ray diffraction pattern of "burnt" area shown in figure 11c)

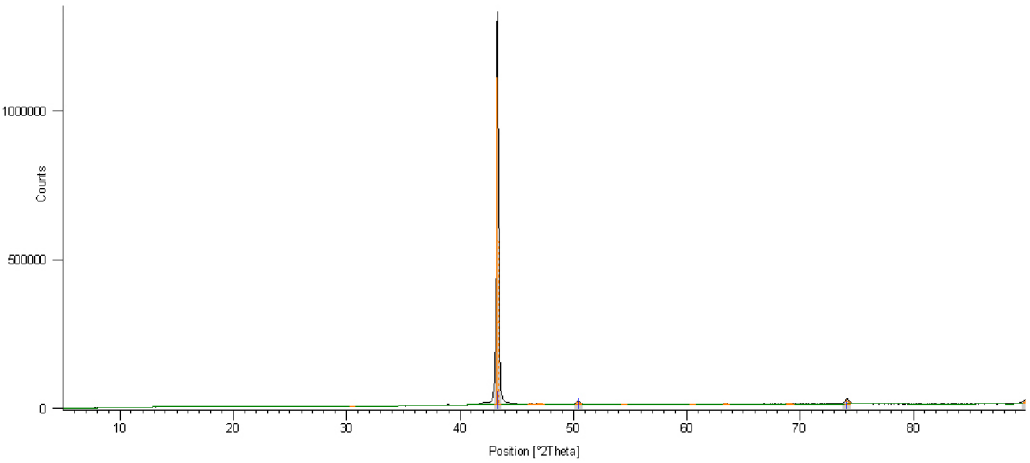

Figure 13: X-ray diffraction pattern of copper top coat of specimen $AZ91_{SEN\text{-}Cu25}$

5.4 Effect of pretreatment process prior copper electroplating

Prior copper electroplating the same pretreatment process as in the case of electroless nickel deposition was applied. The AZ91 specimen coated with 6 μm thick Ni-P coating was immersed in alkaline solution for 20 min at temperature 60 °C. Afterwards, the specimen was washed with distilled water, isopropanol and dried with hot air. The specimen was then immersed in acid pickling solution for approximately 5 s, washed with distilled water, isopropanol and dried with hot air. No changes were visually observed after pretreatment at surface of AZ91 coated with Ni-P.

Pretreated specimen was subjected to copper electroplating. The specimen was labeled as $AZ91_{SEN\text{-}PrCu10}$. In figure 14 (left) can be seen the photograph of $AZ91_{SEN\text{-}PrCu10}$. At the copper surface can be observed several pits, that can be initial spots for corrosion of the AZ91 substrate. Otherwise, the copper coating visually looks good and adherent to substrate. In figure 14 (right) is shown optical microscopy image of cross section of specimen $AZ91_{SEN\text{-}PrCu10}$. As can be seen the deposited Ni-P and Cu layer are homogeneous and no intermediate layers were observed. Both, the Ni-P and Cu coating seem to be adherent and without any discontinuities.

During pretreatment in alkaline solution, the impurities and greases are removed from surface. In addition, acid pickling solution passes through the pores in Ni-P layer and reacts with AZ91 substrate. As a result, these pores are clogged by the reaction products between the substrate and the acid pickling solution. Consequently, the electroplating solution can not penetrate to the substrate and thus a better quality copper coating can be deposited. Moreover, the corrosion properties are slightly improved as is discussed in subsection 5.6.

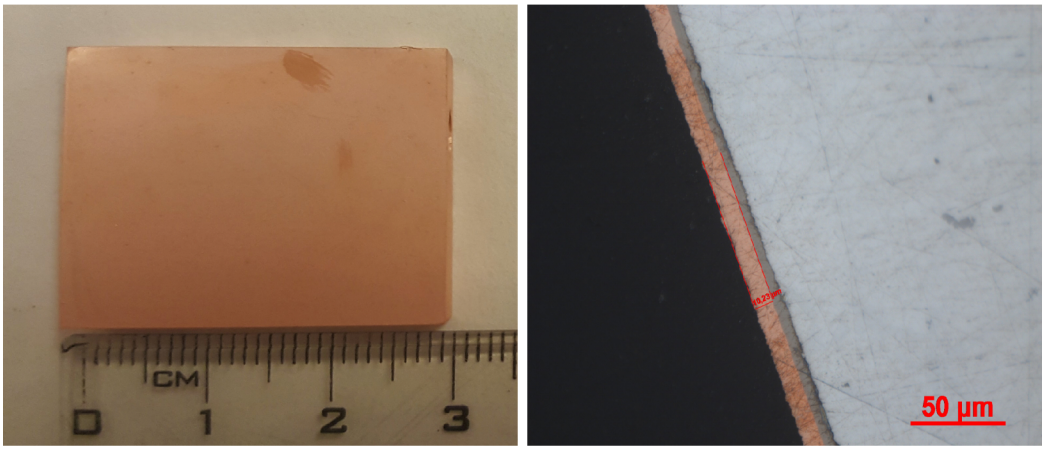

Figure 14: Photograph of specimen $AZ91_{SEN\text{-}PrCu10}$ (left) and optical microscopy image of cross section (right)

5.5 Copper electroplating on duplex Ni-P layers on AZ91

In order to increase corrosion resistance of AZ91 substrate the second Ni-P layer was introduced. The duplex (two) layers Ni-P coating of an entire thickness ∼12 μm was prepared in the same electroless nickeling bath. The pretreatment process was applied in between the two layers. The specimen with duplex ENP coating was labeled as $AZ91_{DEN\text{-}Cu10}$. In figure 15 (left) can be seen photograph of AZ91 with duplex (two) Ni-P layers and copper coating with thickness of 10 μm. Several darker stripes were observed on the surface. It can be caused by hydrogen evolution on the edge, where current density is the highest. The optical microscopy image of cross section is depicted in figure 15 (right). As can be seen the prepared Ni-P and copper coating is homogeneous and their thicknesses were approximately 11 and 10 μm, respectively. No intermediate layer was observed between the substrate and the Ni-P coating, confirming the suitable pretreatment. Also, between Ni-P layer and copper top coat was not observed any intermediate layer and adhesion of copper to Ni-P bond coat is great. No defects were observed in copper or Ni-P coatings.

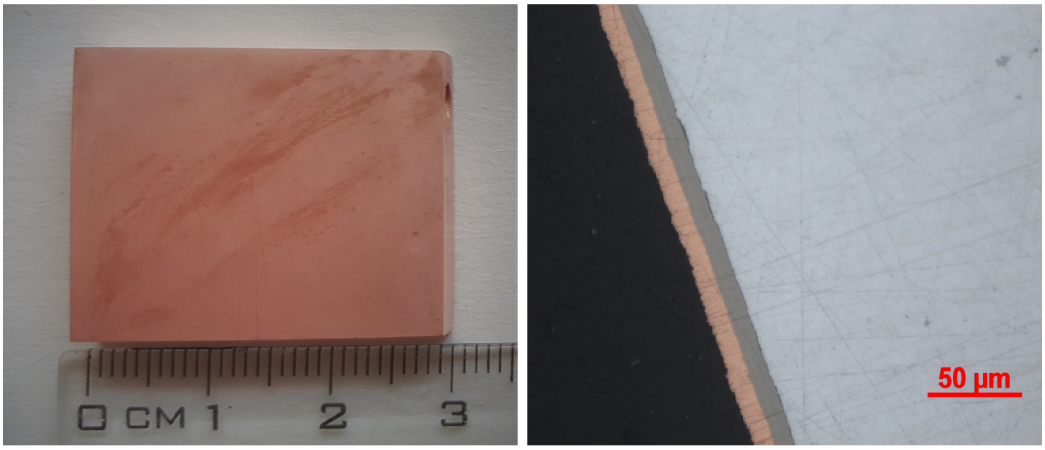

Figure 15: Photograph of specimen $AZ91_{DEN\text{-}Cu10}$ (left) and optical microscopy image of cross section (right)

5.6 Corrosion study of AZ91 coated with Ni-P and Cu

In order to characterize corrosion properties of coated magnesium alloy AZ91 a potentiodynamic polarization test was used. The potentiodynamic polarization test of bare AZ91 and coated AZ91 was performed in 0.1 mol·dm^{-3} NaCl solution in range of -100 mV to 200 mV at a constant voltage scan rate of 1.0 mV·s^{-1}. In figure 16 are shown potentiodynamic polarization curves of bare and coated AZ91 with multi-layer coating systems. As can be seen the corrosion resistance of bare AZ91 substrate is poor due to its heterogeneous structure and thus galvanic coupling between α and β-phase occured. In previous reasearch at Faculty of chemistry BUT [43], the potentiodynamic behaviour of single-layer Ni-P coating on AZ91 was determined. The AZ91 alloy was coated with 10 μm thick ENP layer and for purposes of this thesis it was labeled as AZ91$_{\text{SEN}}$. By introducing the Ni-P layer on AZ91 the corrosion potential is significantly shifted to more positive values. The multi-layer coating systems Ni-P/Cu on AZ91 is further improving corrosion resistance of AZ91 substrate as can be seen in figure 16. The potentiodynamic polarization test results can be found in table 5.

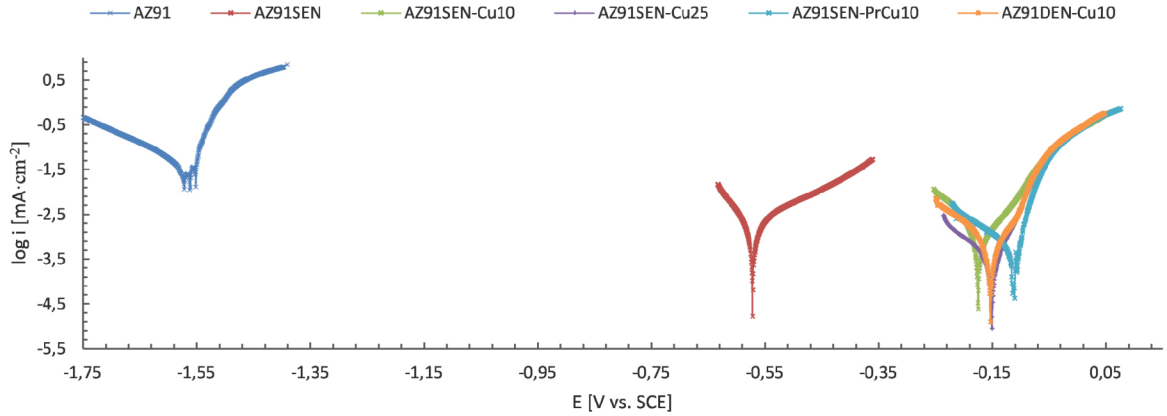

Figure 16: Potentiodynamic polarization curves of bare and coated AZ91 Mg alloy in 0.1 M NaCl solution at a scan rate of 1 mV/s

In figure 17 are depicted potentiodynamic polarization curves of specimens prepared in experimental part of this diploma thesis. Comparing the specimens AZ91$_{\text{SEN-Cu10}}$ and AZ91$_{\text{SEN-Cu25}}$ is evident that corrosion properties were improved by introducing thicker Cu coating. The corrosion current density is improved from 0.823 μAcm^{-2} of AZ91$_{\text{SEN-Cu10}}$ to 0.278 μAcm^{-2} of specimen AZ91$_{\text{SEN-Cu25}}$. By introducing second Ni-P layer (entire thickness of $\sim$12μm) beneath 10 μm thick Cu layer the corrosion current density is slightly reduced in comparison with AZ91$_{\text{SEN-Cu10}}$ to value 0.605 μAcm^{-2}. As can be seen in figure 17 the pretreatment process prior copper electroplating significantly improved corrosion potential. However, the corrosion current density remained at similar values in comparison with AZ91$_{\text{SEN-Cu10}}$ as can be seen in table 5. The copper coating remained intact and did not exfoliate after potentiodynamic test, revealing an excellent adhesion of the coating.

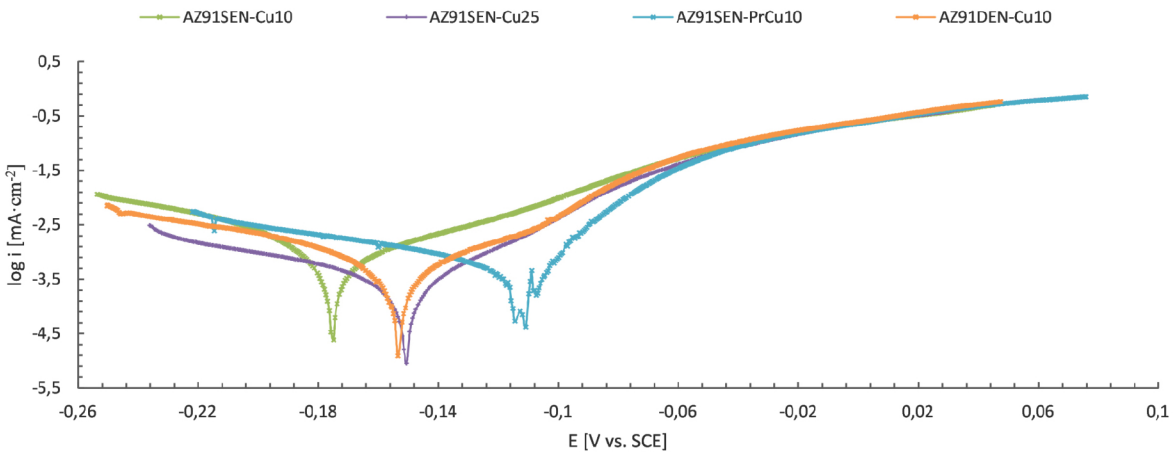

Figure 17: Potentiodynamic polarization curves of coated AZ91 Mg alloy in 0.1 M NaCl solution at a scan rate of 1 mV/s

Table 5: Electrochemical parameters obtained from Ni-P/Cu coating layer on AZ91 substrate

Specimen	E_{corr} [mV vs. SCE]	i_{corr} [μAcm^{-2}]
AZ91 substrate	-1558.3	32.1
$AZ91_{SEN}$ [43]	-590.0	1.4
$AZ91_{SEN\text{-}PrCu10}$	-117.8	0.625
$AZ91_{DEN\text{-}Cu10}$	-142.6	0.605
$AZ91_{SEN\text{-}Cu10}$	-168.6	0.823
$AZ91_{SEN\text{-}Cu25}$	-146.7	0.278

5.7 Coating characterization

In order to fully characterize Ni-P/Cu coating system on Mg alloy AZ91 were prepared two specimens with single-layer 6 μm thick high-phosphorous Ni-P bond-coat. Subsequently, the specimens were used for copper electrodeposition of 10 and 25 μm thick layers. Based on previous research, the initial copper layer was formed at low cathode current density of 0.08 A·dm^{-2}. Afterwards, the cathode current density was increased to 0.4 A·dm^{-2} for 60 and 150 min in order to develop 10 and 25 μm thick Cu coating, respectively. The specimens were labeled as $AZ91_{SEN\text{-}Cu10}$ and $AZ91_{SEN\text{-}Cu25}$.

5.7.1 Hardness measurement

Microhardness of electrodeposited Cu top coat was determined by microhardness tester LECO AMH43 using Vickers method. The load was set to 10 gf with a duration of 10 s. Due to thin Ni-P layer the load was set to 5 gf with a same duration. In previous research in BUT the average hardness of AZ91 substrate was determined. Measurement was performed at a load 1 kg due to the presence of phases with different hardness and average hardness value is 70 ± 10 HV_1 [44]. The Dean-Dixon test was used to assess the results and exclude different values. The individual measurement deviation was set to 2σ to include 95% of the values. Measured values of microhardness of Ni-P bond coat and copper coating can be seen in table 6.

Table 6: Microhardness values of Ni-P bond coat and Cu top coat

Measurement	Ni-P [$HV_{0.005}$]	Cu [$HV_{0.01}$]
1	400	205
2	425	207
3	416	208
4	411	207
5	408	205
6	403	209
Arithmetic average	411	207
Standart deviation	± 10	± 2

Moreover, hardness of surface was determined at specimens coated with 10 and 25 μm thick copper coating. Hardness measurement was performed at a load 0.5 kg and 2 kg. The results of surface hardness measurement can be found in table 7. As can be seen the surface hardness values of specimen $AZ91_{SEN\text{-}Cu10}$ is higher due to influence of harder Ni-P bond coat beneath 10 μm thick Cu layer. The measurement of surface hardness was done in order to determine the "real" hardness of surface. As can be seen, the Ni-P bonding coat protects the softer magnesium alloy, which will withstand greater mechanical stress in many application, such as car body.

Table 7: Surface hardness of specimens $AZ91_{SEN\text{-}Cu10}$ and $AZ91_{SEN\text{-}Cu25}$

	$AZ91_{SEN\text{-}Cu10}$		$AZ91_{SEN\text{-}Cu25}$	
Measurement	$HV_{0.5}$	HV_2	$HV_{0.5}$	HV_2
1	137	99	113	83
2	122	108	106	89
3	126	100	104	87
4	129	107	107	86
5	136	104	102	87
6	124	105	108	85
Arithmetic average	129	104	107	86
Standart deviation	± 6	± 4	± 4	± 2

5.7.2 Optical microscopy

The cross section of specimens $AZ91_{SEN\text{-}Cu10}$ and $AZ91_{SEN\text{-}Cu25}$ was studied using optical microscopy. It can be seen in the figures 18, 19 that the Ni-P coating had good adhesion to the substrate surface, without visible discontinuities or undesirable interlayer. Furthermore, optical microscope was used in order to determine thicknesses of individual coatings. Average thickness of Ni-P layer was determined to be 5.7 ± 0.6 μm. Average thickness of Cu top coat was determined to be 11.0 ± 1.1 μm at specimen $AZ91_{SEN\text{-}Cu10}$. In a similar way was measured thickness of Ni-P bond coat and Cu top coat at specimen $AZ91_{SEN\text{-}Cu25}$. Average thickness of Ni-P coating and Cu top coat is 5.6 ± 0.7 μm and 25.2 ± 1.8 μm, respectively.

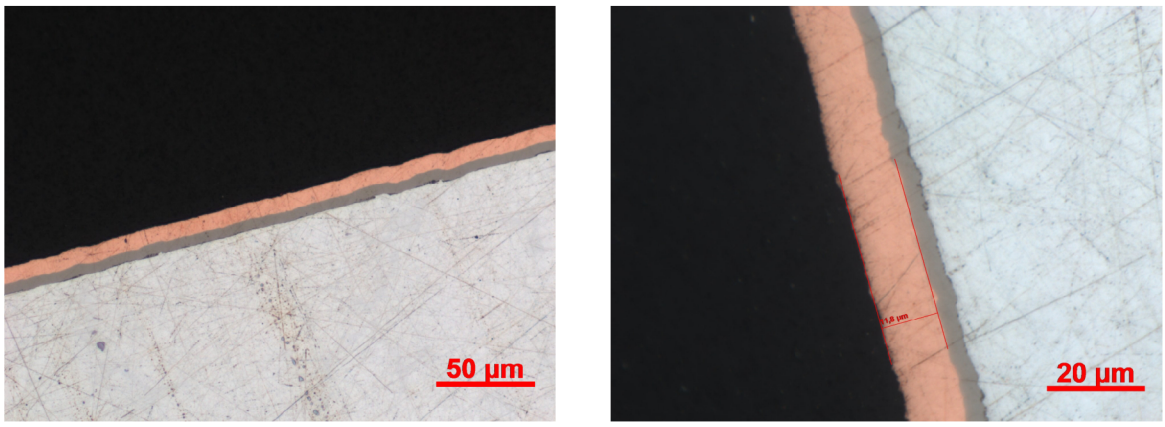

Figure 18: Optical microscopy cross section images of specimen $AZ91_{SEN\text{-}Cu10}$

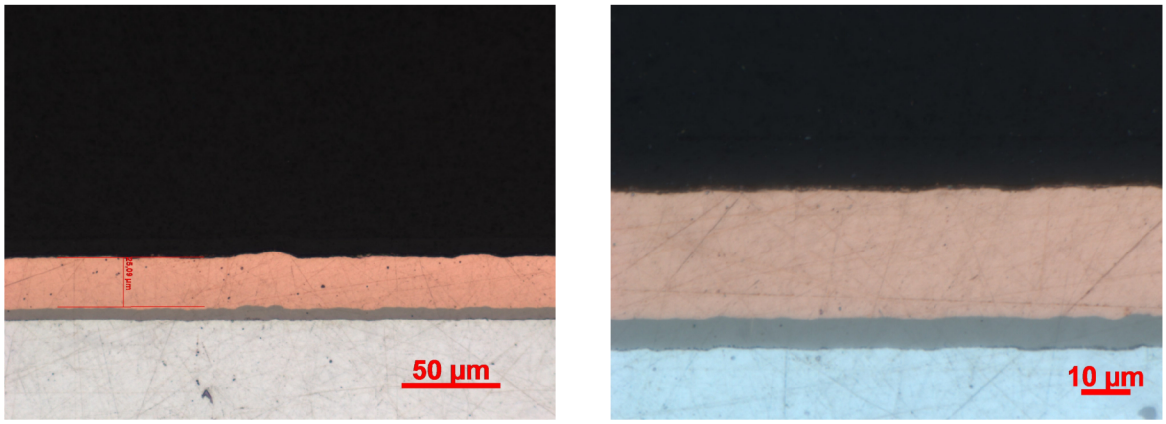

Figure 19: Optical microscopy cross section images of specimen $AZ91_{SEN\text{-}Cu25}$

5.7.3 Scanning electron microscopy

SEM was used for cross section characterization of specimen $AZ91_{SEN\text{-}Cu25}$. The scanning electron microscopy characterization was performed under conditions described in subsection 4.6.4. Similarly to OM observation, in figure 20 can be seen that the Ni-P coating has good adhesion to the AZ91 substrate. Also, the Ni-P coating covers the substrate surface equally. The copper top coat has good adhesion to Ni-P coating. Furthermore, no defects were observed in Ni-P and Cu coatings. In figure 20 (right) can be seen backscatter electron image of specimen $AZ91_{SEN\text{-}Cu25}$. The interface between Ni-P and Cu coating is hard to see due to little difference of atomic number of Ni and Cu.

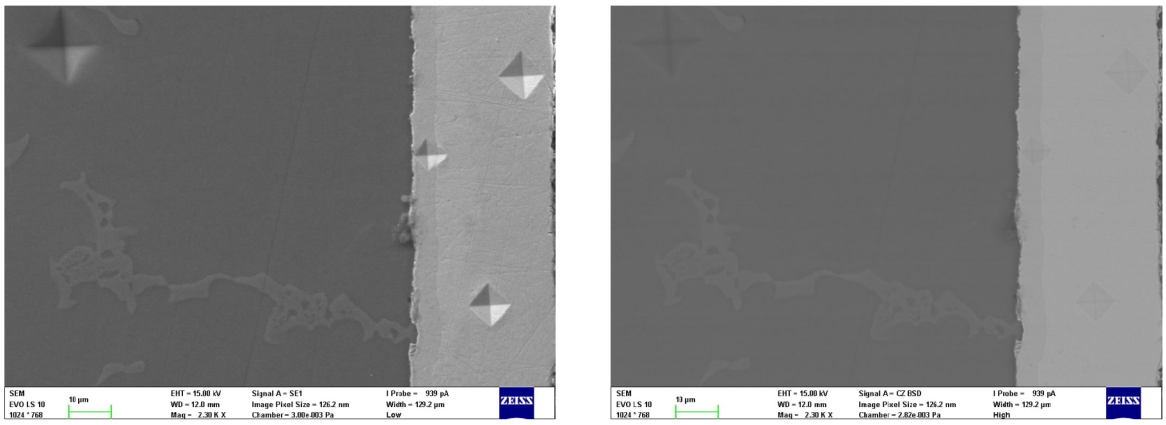

Figure 20: Cross sectional secondary electron (SE) image (left) and backscattered electron (BSE) image (right) of magnesium alloy AZ91 coated with Ni-P and Cu

5.7.4 Elemental analysis of coatings

Using scanning electron microscopy with energy dispersive X-ray detector, the morphology and elemental composition of Ni-P/Cu coatings on magnesium alloy AZ91 were examined. The analysis was performed under conditions described in subsection 4.6.4. In figure 21 (left) can be seen SEM image of cross section of AZ91 coated with 6 μm thick Ni-P bond-coat and 25 μm thick copper top coat. The element mapping of this area is shown in figure 21 (right).

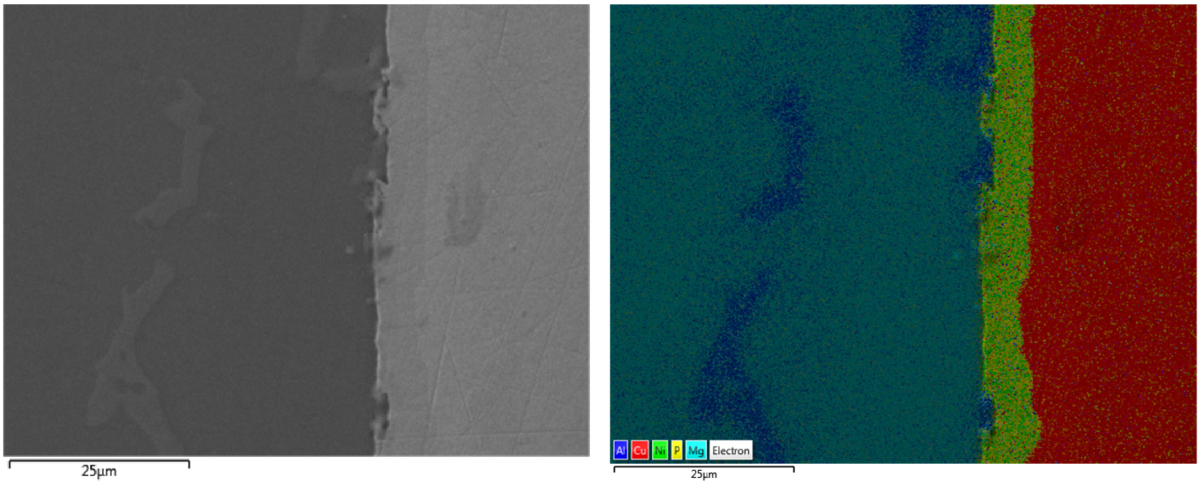

Figure 21: SEM picture (left) and elemental mapping (right) of cross section of magnesium alloy AZ91 coated with Ni-P and Cu

Furthermore, the layout of elements Mg, Al, Ni, P and Cu is shown in figure 22. As can be seen there is sharp interface between individual coatings. Both, nickel and phosphorous are equally distributed over its entire cross section. In figure 22a) and b) is evident the presence of intermetallic $Mg_{17}Al_{12}$ β-phase, where the Al content is higher in comparison with surrounding solid solution.

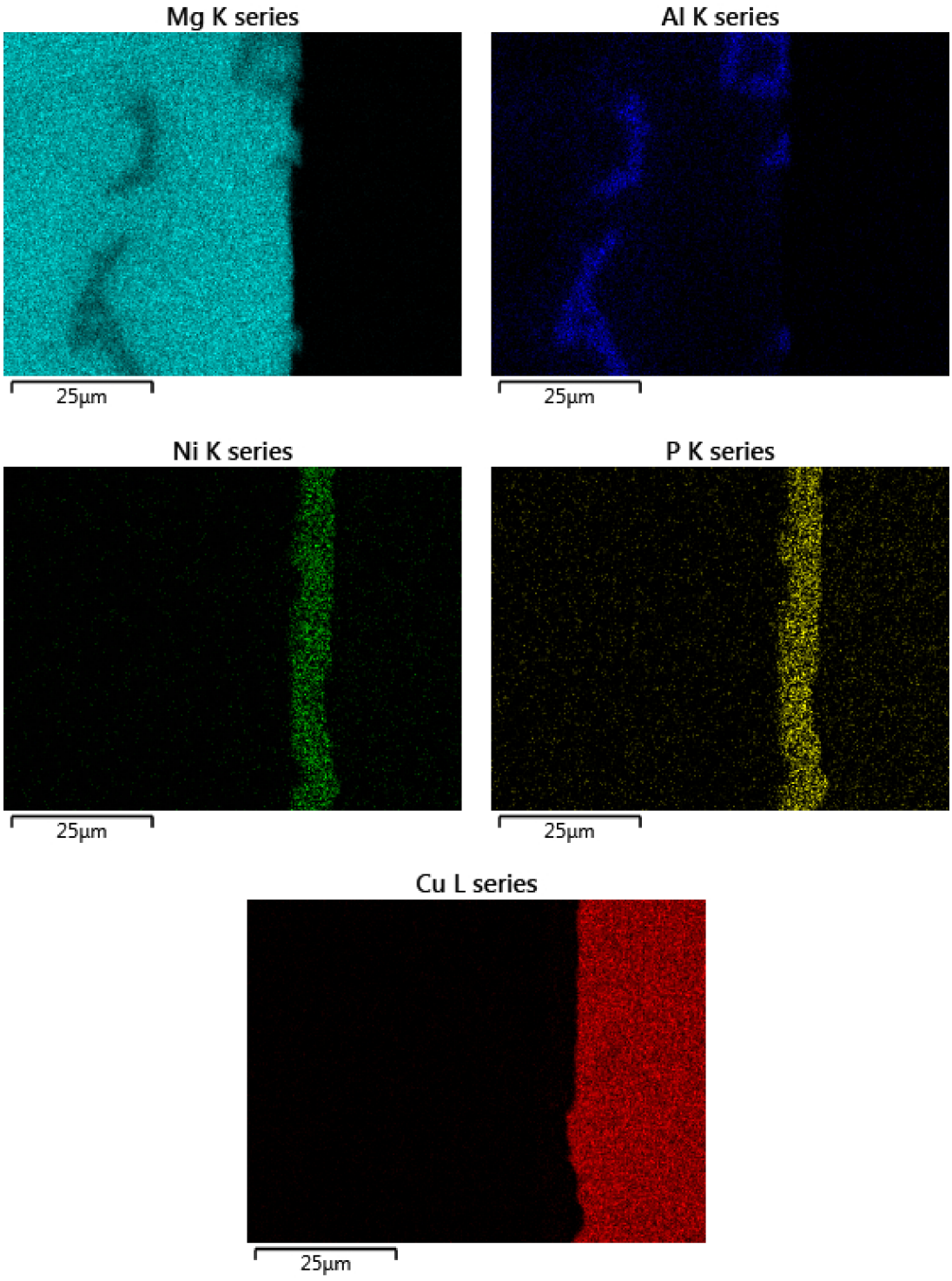

Figure 22: Mapping of individual elements

Figure 23 shows marked areas for EDX analysis in order to obtain information about element composition of AZ91 substrate, Ni-P bond coat and copper top coat. Results of EDX analysis of spectrum 1-7 is shown in figure 24. As was mentioned above the aluminium content in intermetallic $Mg_{17}Al_{12}$ phase (Spectrum 2) is higher than in surrounding α-phase (Spectrum 1) Average element content in deposited Ni-P bond coat is 11.2 wt.% of phosphorous and 88.8 wt.% of nickel. It was determined that there are no impurities in copper top coat and copper average content is 100 wt.%. The average element composition of spectrum 1-7 in weight percentage can be seen in table 8.

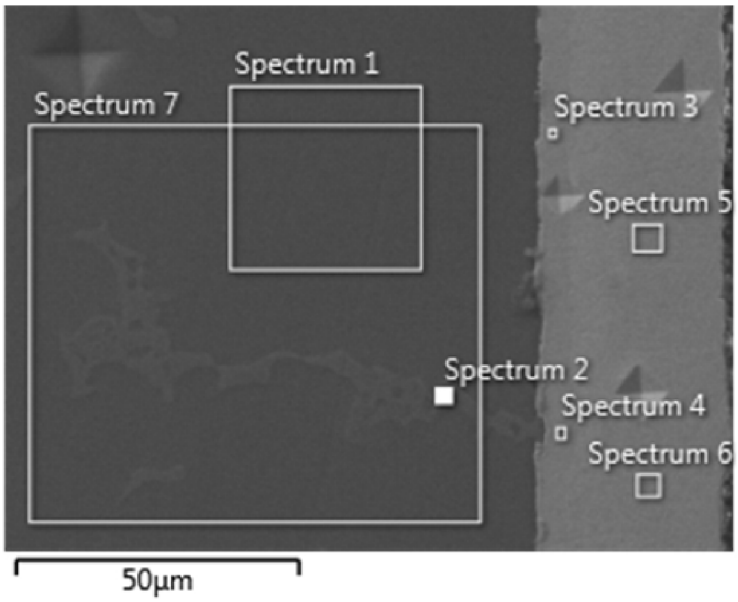

Figure 23: Marked areas for EDX analysis of spectrum 1-7

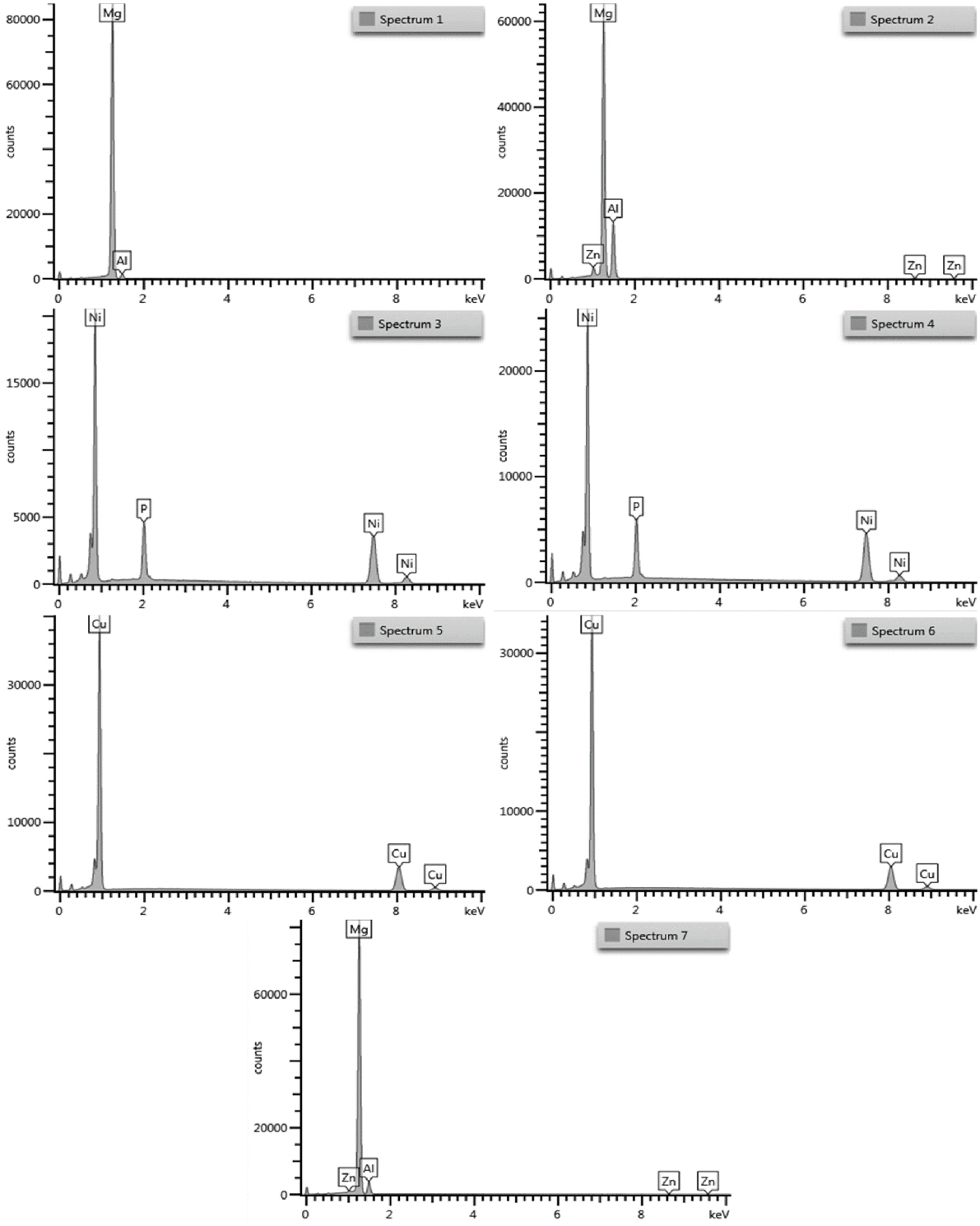

Figure 24: The output EDS analysis spectrum of areas 1-7 from figure 23

Table 8: Element composition of areas shown in figure 23 determined by EDX analysis

Spectrum	Al [wt.%]	Cu [wt.%]	Mg [wt.%]	Ni [wt.%]	P [wt.%]	Zn [wt.%]
1	4.1	—	95.9	—	—	—
2	29.0	—	67.2	—	—	3.8
3	—	—	—	88.8	11.2	—
4	—	—	—	88.8	11.2	—
5	—	100.0	—	—	—	—
6	—	100.0	—	—	—	—
7	10.5	—	88.5	—	—	1.0

In figure 25 is depicted SEM image showing a scan line for EDX analysis. The line scan was performed over α-phase and intermetallic $Mg_{17}Al_{12}$ phase in AZ91 magnesium alloy, nickel-phosphorous bond coat and copper top coat. In figure 26 can be seen profiles of individual elements in weight percentage over entire cross section. The aluminium and zinc content increase over intermetallic $Mg_{17}Al_{12}$ phase, whereas magnesium content decreases. Then, the aluminium content is decreasing up to interface AZ91-ENP. The zinc in α-phase and individual coatings is only trace amounts. As can be seen, there are sharp interfaces between AZ91 substrate and ENP layer and Cu top coat.

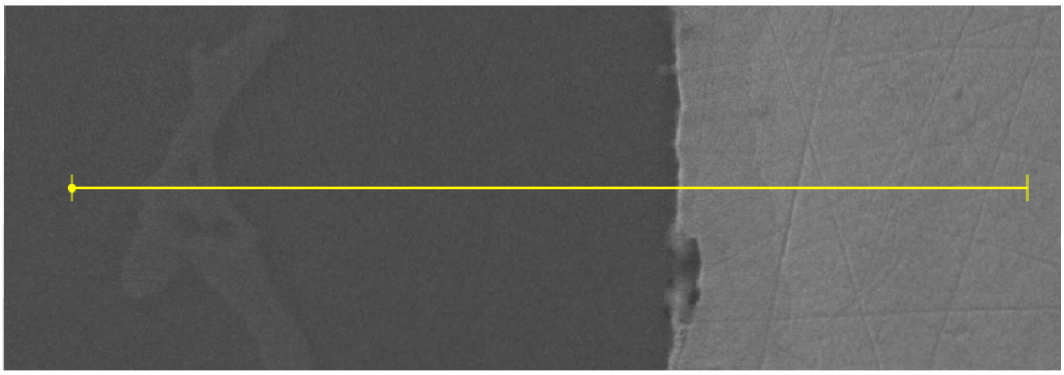

Figure 25: Picture taken by scanning electron microscopy (SEM) showing a scan line for EDX analysis over AZ91, Ni-P bond coat and copper coating

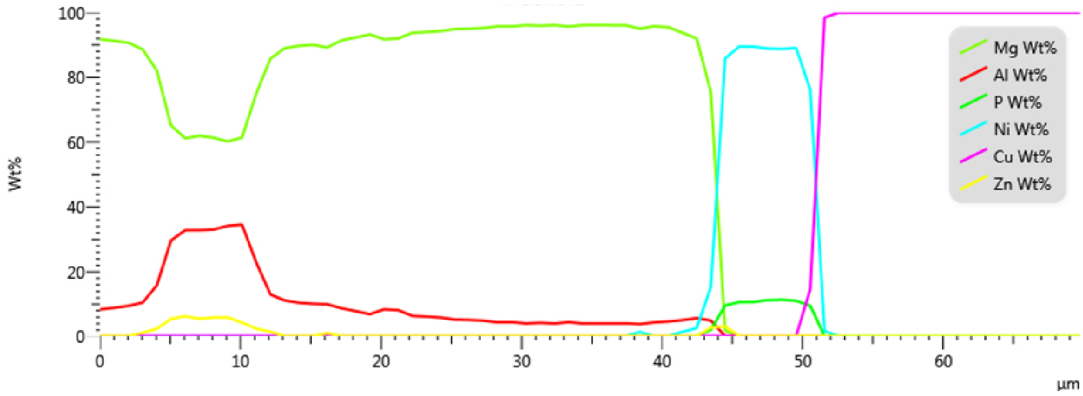

Figure 26: Profiles of individual elements in wt.% in line scan analysis over entire cross section depicted in figure 25

6 Summary of Experimental Part and Discussion

6.1 Electrodeposition of copper on AZ91 coated with Ni-P

The electroplating was found feasible on the AZ91 magnesium alloy covered with high-phosphorous Ni-P bond coat. In order to obtain high quality copper coating, the initial layer formation at low cathode current density of 0.08 $A \cdot dm^{-2}$ is crucial. Afterwards, it is possible to increase the cathode current density up to 0.4 $A \cdot dm^{-2}$. By further increasing the cathode current density the dark orange "burnt" areas appeared. Furthermore, it was found that a 6 μm thick layer provides sufficient protection of the AZ91 substrate for copper electroplating from cyanide bath.

To reduce porosity of Ni-P coating and simultaneously improve quality of galvanic copper coating on magnesium alloy AZ91 coated with Ni-P, the pretreatment process prior electroplating was applied. This resulted in clogging of the pores in the Ni-P coating and preventing the plating solution from accessing the substrate. By introducing the second Ni-P layer resulted in coverage of pores in first Ni-P layer and thus the quality of copper top coat was improved. This suggests that if a suitable pretreatment process prior to plating is selected, a second Ni-P layer is not needed to increase AZ91 substrate protection. Apparently, it would be possible to use magnesium alloys coated with lower thickness of Ni-P bond coat for copper electroplating. It can be very promising for use in industrial practice.

6.2 Corrosion resistance of coated AZ91 magnesium alloy

Table 9 shows comparison of corrosion properties of coated AZ91 with various coating systems prepared in this work and in selected literature. As can be seen the specimen $AZ91_{SEN\text{-}Cu25}$ exhibit the lowest corrosion current density of 0.278 $\mu A \cdot cm^{-2}$ and it is more than 2 times better compared to samples prepared at work [45]. The authors H.Yang et al. used zinc immersion pretreatment with following Cu pre-plating process. Subsequently, approximately 15 μm thick Ni layer was electrodeposited. But the authors performed measurements in 3.5 wt.% NaCl solution, which is more aggressive and corrosive current density values may be higher. By comparing samples $AZ91_{SEN\text{-}Cu25}$ and $AZ91_{DEN20\text{-}Ni15}$, a significant improvement in the corrosion properties of sample $AZ91_{SEN\text{-}Cu25}$ can be seen, which has even a lower coating system thickness. As already mentioned, by introducing double-layer Ni-P coating on AZ91 there is no significant improvement of corrosion current density in comparison with pretreated specimen $AZ91_{SEN\text{-}PrCu10}$. This indicates that a suitable pretreatment can significantly accelerate the plating process of magnesium alloys in industrial practice while maintaining corrosion properties.

Table 9: Comparison of corrosion properties of coated AZ91 specimens with literature

Specimen	E_{corr} [mV vs. SCE]	i_{corr} [μA·cm^{-2}]	Reference
$AZ91_{SEN\text{-}Cu25}$	-146.7	0.278	This work
$AZ91_{SEN\text{-}PrCu10}$	-117.8	0.625	This work
$AZ91_{DEN\text{-}Cu10}$	-142.6	0.605	This work
$AZ91_{DEN20\text{-}Ni15}$	-283.3	0.750	[40]
Ni-coated AZ91D	-248.0	0.600	[45]

6.3 Characterization of prepared coating systems on AZ91 substrate

After preparation of the metallographic cut and subsequent polishing of the sample, the thickness of the individual layers of the coating was measured using an optical microscope. The prepared coatings have good adhesion and there were no undesirable interlayers or discontinuities. It can be said that prepared coatings on AZ91 substrate were defect free. In addition, elemental analysis was performed using EDX analysis. Average elemental composition of individual coatings and AZ91 substrate can be found in table 8. By elemental mapping and line scan over entire cross section was observed sharp interfaces between AZ91 substrate, Ni-P bond coat and Cu top coat (Figures 22, 26).

7 Conclusion

In this diploma thesis was described preparation and characterization of multi-layer coating system Ni-P/Cu for coating of magnesium alloy AZ91. Using scanning electron microscopy and optical microscopy was observed,that prepared Ni-P and Cu coating have good adhesion and coatings are defect free without any discontinuities or undesirable interlayers. In terms of elemental composition, the prepared coatings on AZ91 were homogeneous. The microhardness was determined for both Ni-P and Cu coatings. Their average values are 411 ± 10 $HV_{0.005}$ and 207 ± 2 $HV_{0.01}$, respectively. Furthermore, the hardness of specimen surface was determined (Table 7).

In conclusion, the main points that were included in the pretreatment and subsequent electrodeposition of copper can be summarized:

• The low-phosphorous Ni-P coating does not provide sufficient corrosion protection of AZ91 substrate for further copper electroplating.

• It was determined the lowest thickness of Ni-P bond coat on AZ91 substrate suitable for copper electroplating. Its thickness is approximately 6 μm.

• The formation of initial copper layer at low current densities is crucial in order to obtain defect free copper top coat. It was found that current density can not exceed 0.4 $A \cdot dm^{-2}$ otherwise "burnt" areas would occur.

• The appropriate pretreatment process prior electroplating may improve the corrosion properties of magnesium alloy AZ91.

• The prepared specimens were subjected to potentiodynamic polarization test. The corrosion resistance of electrodeposited copper is significantly enhanced by introducing 25 μm thick copper layer and it offers the lowest value of corrosion current density ($\sim 0.278\ \mu A \cdot dm^{-2}$).

Based on this knowledge, I would like to propose possible topics for other bachelor's or master's theses that would complement and follow up on the current research in the field of galvanic plating of magnesium alloys:

• Effect of pretreatment prior electroplating of magnesium alloy coated with Ni-P

• Electroplating of nickel and chromium on AZ91 coated with Ni-P/Cu bond coats

• Electroplating of copper from pyrophosphate bath on AZ91 coated with Ni-P

It can be said, that the stated objectives of the diploma thesis have been fulfilled.

8 List of Abbreviations and Symbols

at.%	Atomic percentage
AZ31	Magnesium alloy
AZ91	Magnesium alloy
BSE	Backscatter electron
EDX	Energy dispersive x-ray spectroscopy
$\mathbf{E_{corr}}$	Corrosion potential
EIS	Electrochemical impedance spectroscopy
ENP	Electroless nickel-phosphorous
gf	Gram force
GDOES	Glow-discharge optical emission spectroscopy
HV	Vickers hardness
$\mathbf{I_{corr}}$	Corrosion current
Ni-P	Nickel-phosphorous
OM	Optical microscopy
SCE	Saturated calomel electrode
SE	Secondary electron
SEM	Scanning electron microscopy
wt.%	Weight percentage
XRD	X-ray diffraction

References

[1] Liping Wu, Zhongdong Yang, and Gaowu Qin. Kinetic study of a novel electroless nip deposition on az91d magnesium alloy using nickel hypophosphite as the metal salt. *Journal of Alloys and Compounds*, 694:1133 – 1139, 2017.

[2] Elsa Georgiza, Jelica Novakovic, and Panayota Vassiliou. Characterization and corrosion resistance of duplex electroless ni-p composite coatings on magnesium alloy. *Surface and Coatings Technology*, 232:432 – 439, 2013.

[3] J.E. Gray and B. Luan. Protective coatings on magnesium and its alloys — a critical review. *Journal of Alloys and Compounds*, 336(1):88 – 113, 2002.

[4] Xiaomin ; Keong K G Sha, W ; Wu. *Electroless Copper and Nickel-Phosphorus Plating: Processing, Characterisation and Modelling*. Woodhead Publishing Series in Metals and Surface Engineering. Elsevier Science, 2011.

[5] Roy Johnsen. Plating and chemical coatings. Norwegian University of science and technology lecture, 2018.

[6] Mordechay Schlesinger and Milan Paunovic. *Modern Electroplating*. John Wiley and Sons Ltd, 5th ed. edition, 2010.

[7] B.L Mordike and T Ebert. Magnesium: Properties — applications — potential. *Materials Science and Engineering: A*, 302(1):37 – 45, 2001.

[8] Jaromír Drápala and rafinace a recyklace Vysoká škola báňská Technická univerzita Ostrava. Katedra neželezných kovů. *Hořčík, jeho slitiny a binární systémy hořčík - příměs = Magnesium, its alloys and Mg - admixture binary systems*. Vysoká škola báňská - Technická univerzita, 1. vyd. edition, 2004.

[9] H.Y. Yang, X.B. Chen, X.W. Guo, G.H. Wu, W.J. Ding, and N. Birbilis. Coating pretreatment for mg alloy az91d. *Applied Surface Science*, 258(14):5472 – 5481, 2012.

[10] Li ping WU, Jing jing ZHAO, Yong ping XIE, and Zhong dong YANG. Progress of electroplating and electroless plating on magnesium alloy. *Transactions of Nonferrous Metals Society of China*, 20:s630 – s637, 2010.

[11] G. S Frankel M. Stratmann. *Corrosion and oxide films*. Weinheim: Wiley-VCH, 1. vyd. edition, 2003.

[12] Jakub Tkacz. *Korozní odolnost konstrukčních slitin hořčíku*. Disertační práce, Vysoké učení technické v Brně. Fakulta chemická. Centrum materiálového výzkumu, 2014.

[13] Andrej Atrens, Guang-Ling Song, Ming Liu, Zhiming Shi, Fuyong Cao, and Matthew S. Dargusch. Review of recent developments in the field of magnesium corrosion. *Advanced Engineering Materials*, 17(4):400–453.

[14] Teng-Shih Shih, Jyun-Bo Liu, and Pai-Sheng Wei. Oxide films on magnesium and magnesium alloys. *Materials Chemistry and Physics*, 104(2):497 – 504, 2007.

[15] Denny A Jones. *Principles and prevention of corrosion*. Prentice Hall, Upper Saddle River, NJ, 2nd ed edition, c1996.

[16] S Mathieu, C Rapin, J Steinmetz, and P Steinmetz. A corrosion study of the main constituent phases of az91 magnesium alloys. *Corrosion Science*, 45(12):2741 – 2755, 2003.

[17] Nahed El Mahallawy, L. K. Meena, S. K. Tiwari, and Raghuvir Singh. Surface treatment of magnesium alloys by electroless Ni–P plating technique with emphasis on zinc pretreatment. *Key Engineering Materials*, 384(2):241–262, 2008.

[18] Zhongcai Shao, Zhiqiang Cai, Rong Hu, and Shouqiang Wei. The study of electroless nickel plating directly on magnesium alloy. *Surface and Coatings Technology*, 249:42 – 47, 2014.

[19] Zhi-Hui Xie, Fang Chen, Shu-Rong Xiang, Jun-Li Zhou, Zheng-Wei Song, and Gang Yu. Studies of several pickling and activation processes for electroless ni-p plating on az31 magnesium alloy. *Journal of The Electrochemical Society*, 162(3):D115–D123, 2014-12-11.

[20] X. SHU, Y. WANG, J. PENG, P. YAN, B. YAN, X. FANG, and Y. XU. Recent progress in electroless Ni coatings for magnesium alloys. *International Journal of Electrochemical Science*, 10(10):1261–1273, 2015.

[21] Fakiha El-Taib Heakal, Madiha A. Shoeib, and Maanoum A. Maanoum. Optimizing parameters affecting electroless Ni-P coatings on az91d magnesium alloy as corrosion protection barriers. *Protection of Metals and Physical Chemistry of Surfaces*, 53(1):177–187, Jan 2017.

[22] Charu Singh, L. K. Meena, S. K. Tiwari, and Raghuvir Singh. Establishing environment friendly surface treatment for AZ91 magnesium alloy for subsequent electroless nickel plating. *Journal of The Electrochemical Society*, 165(2):C71–C85, 2018-01-25.

[23] Jothi Sudagar, Jianshe Lian, and Wei Sha. Electroless nickel, alloy, composite and nano coatings – a critical review. *Journal of Alloys and Compounds*, 571:183 – 204, 2013.

[24] Roy Parkinson. Properties and applications of electroless nickel. *Nickel Development Institute Technical Series no.10081*, 1, 1995.

[25] Hajdu Juan B. Mallory, Glenn O. *Electroless Plating - Fundamentals and Applications*. William Andrew Publishing/Noyes, 1990.

[26] C. A. Loto. Electroless nickel plating – a review. *Silicon*, 8(2):177–186, Apr 2016.

[27] B.-H. Chen, L. Hong, Y. Ma, and T.-M. Ko. Effects of surfactants in an electroless nickel-plating bath on the properties of Ni-P alloy deposits. *Industrial & Engineering Chemistry Research*, 41(11):2668–2678, 2002.

[28] R. Elansezhian, B. Ramamoorthy, and P. Kesavan Nair. Effect of surfactants on the mechanical properties of electroless Ni–P coating. *Surface and Coatings Technology*, 203(5):709 – 712, 2008. Proceedings of the 35th International Conference on Metallurgical Coatings and Thin Films.

[29] W. Riedel. *Electroless Nickel Plating.* ASM International, 1991.

[30] P. Hersch. *Transactions of the Institute of Metal Finishing*, 51:417, 1955 - 1956.

[31] J. Bielinski. Untersuchugen zur optinierugn von loesunger zur chemischen vernickeling. *Metalloberfläche*, 38(2):60 – 65, 1984.

[32] G Cavallotti, P.; Salvago. Studies on chemical reduction of nickel and cobalt by hypophosphite ii. characteristics of the process. *Electrochimica Metallorum*, 3:239 – 266, 1968.

[33] A. Randin, J. P.;Hintermann. Calorimetric study of the electroless deposition of nickel. *The Electrochemical Society*, 117(2):160 – 167, 1970.

[34] R. C. Agarwala and Vijaya Agarwala. Electroless alloy/composite coatings: A review. *Sadhana*, 28(3):475–493, Jun 2003.

[35] H. Ashassi-Sorkhabi and S.H. Rafizadeh. Effect of coating time and heat treatment on structures and corrosion characteristics of electroless ni–p alloy deposits. *Surface and Coatings Technology*, 176(3):318 – 326, 2004.

[36] K. G. Keong W. Sha, Xiaomin Wu. *Electroless copper and nickel–phosphorus plating.* Elsevier Ltd, 2011.

[37] F. C. Campbell. *Metals fabrication.* ASM International, Materials Park, Ohio, 2013.

[38] Vladimír Ruml. *Galvanické pokovování.* SNTL, Praha, vyd. 1. edition, 1981.

[39] Nguyen Van Phuong, Min-Sik Park, Chang Dong Yim, Bong Sun You, and Sungmo Moon. Corrosion protection utilizing ag layer on cu coated az31 mg alloy. *Corrosion Science*, 136:201 – 209, 2018.

[40] Charu Singh, S.K. Tiwari, and Raghuvir Singh. Exploring environment friendly nickel electrodeposition on az91 magnesium alloy: Effect of prior surface treatments and temperature of the bath on corrosion behaviour. *Corrosion Science*, 151:1 – 19, 2019.

[41] Martin Žilinský. *Charakterizace tepelně zpracovaných Ni-P povlaků s různými obsahy fosforu.* Bakalářská práce, Vysoké učení technické v Brně, Fakulta chemická. Ústav chemie materiálů, 2018.

[42] Martin Buchtík. *Příprava povlaků na bázi Ni-P na tvářených hořčíkových slitinách.* Diplomová práce.

[43] Roman Brescher. *Příprava a charakterizace Ni-P povlaku na lité hořčíkové slitině AZ91.* Bakalářská práce, Vysoké učení technické v Brně, Fakulta chemická, 2018.

[44] Tomáš Najser. *Studium mikrostruktury deponovaných Ni-P povlaků s různými obsahy fosforu.* Bakalářská práce, Vysoké učení technické v Brně, Fakulta chemická, 2018.

[45] Haiyan Yang, Xingwu Guo, Xiaobo Chen, and Nick Birbilis. A homogenisation pretreatment for adherent and corrosion-resistant ni electroplated coatings on mg-alloy az91d. *Corrosion Science*, 79:41 – 49, 2014.